

**THERMAL-STRUCTURAL  
EVALUATION OF  
Ti-6Al-4V  
THERMAL PROTECTION  
SYSTEM PANELS**

By H. L. Eidinoff and L. Rose

Prepared under Contract No. NAS 1-12277 by  
Grumman Aerospace Corporation  
Bethpage, New York 11714

for

NATIONAL AERONAUTICS AND SPACE ADMINISTRATION

## FOREWORD

The work reported herein was performed by the Grumman Aerospace Corporation under NASA Langley Research Center Contract No. NAS 1-12277 - testing and evaluation of two TD Ni-20Cr Thermal Protection System Panels. The technical representatives of the contracting officer were Mr. B. A. Stein of the Materials Research Branch, Materials Division, and Mr. H. L. Bohon of the Thermal Protection Section, Thermal Structures Branch, Structures and Dynamics Division. The period of performance was for seven months, starting in June, 1973.

Many individuals at Grumman contributed to the work reported here. Messrs. Charles Walthers and Barry Bell of the Grumman Environmental Test Group designed the heating array and supervised the testing. Mr. George Myers of Structural Test designed the mechanical loading device and supervised its installation. Much of the testing was performed by Mr. Richard Ewing of the Environmental Test Laboratory. Mr. Carl Salhofen was the instrumentation engineer.

Technical information regarding the panel was provided by Messrs. C. Picard and D. Chaumette of Avions Marcel Dassault. Mr. M. Piry of Grumman provided valuable liaison between Grumman and Dassault.

## CONTENTS

1	SUMMARY . . . . .	1
2	INTRODUCTION . . . . .	2
3	PANEL CONCEPT . . . . .	5
	3.1 Design Criteria . . . . .	5
	3.2 Heat-Shield Materials . . . . .	6
	3.3 Configuration . . . . .	7
	3.4 Unit Weight . . . . .	8
	3.5 Insulation Concepts . . . . .	9
	3.6 Fabrication & Joining Concepts . . . . .	10
4	TEST APPARATUS & PROCEDURES . . . . .	26
	4.1 Heating & Loading Equipment . . . . .	26
	4.2 Instrumentation . . . . .	27
	4.3 Procedures & Test Sequences . . . . .	28
5	RESULTS & DISCUSSION . . . . .	37
	5.1 Initial Thermal Cycles . . . . .	37
	5.2 Thermal-Structural Cycles . . . . .	38
	5.2.1 Panel Thermal Response . . . . .	38
	5.2.2 Flatness Measurements . . . . .	39
	5.2.3 Additional Test Results . . . . .	41
	5.3 Post-Test Inspection . . . . .	42
6	CONCLUSIONS . . . . .	66
7	RECOMMENDATIONS FOR IMPROVED PANEL PERFORMANCE . . . . .	67
8	REFERENCES . . . . .	68
Appendix		
	FLATNESS SURVEY DATA . . . . .	71

## ILLUSTRATIONS

3-1	Grumman H-33 Orbiter Isotherms . . . . .	11
3-2	Ascent Trajectory Parameters . . . . .	12
3-3	Ascent Trajectory Parameters . . . . .	13
3-4	Reentry T rajjectory Parameters . . . . .	14
3-5	Reentry Pressure & Temperature . . . . .	15
3-6	Ascent Pressure Test Condition . . . . .	16
3-7	Reentry Pressure & Temperature Test Conditions . . . . .	17
3-8	Test Article . . . . .	18
3-9	Grumman/Dassault TPS Panel Design . . . . .	21
3-10	Expansion Joint Detail . . . . .	22
3-11	Insulation Specific Conductivity . . . . .	23
3-12	Panel Insulation System . . . . .	24
4-1	Thermal-Structural Test Facility . . . . .	30
4-2	Thermal-Structural Test Facility Control Systems . . . . .	31
4-3	Whiffle-Tree Loading Device . . . . .	32
4-4	Loading-Wire-Number Locations . . . . .	33
4-5	Instrumentation . . . . .	35
4-6	Measuring Bridge . . . . .	36
5-1	Maximum Surface Temperatures Map . . . . .	45
5-2	Frontface Temperature Response . . . . .	46
5-3	Insulation Temperature Response - Effect of Thermal Cycling . . . . .	47
5-4	Temperature Response Through Insulation - Cycle No. 2 . . . . .	48
5-5	Support Rib Temperature Response . . . . .	49
5-6	Effect of Inserting Loading Wires on Insulation Temperature Response . . . . .	50
5-7	Effect of Repeated Reentry Cycles on Insulation Temperature Response . . . . .	51
5-8	Dassault-Installed & Floating Thermocouple Comparison, Run 15 . . . . .	52
5-9	Loading Deflection Survey, Flat No. 7, Midspan . . . . .	53

## ILLUSTRATIONS (cont)

5-10	Permanent Deflection, Midspan . . . . .	54
5-11	Permanent Deflection, Flat No. 4 . . . . .	55
5-12	Maximum Deflection, Limit Room Temperature Pressure Plus 100-Cycle Permanent Set . . . . .	56
5-13	Surface Crack After 88 Cycles . . . . .	60
5-14	Test Article in Fixture After 100 Cycles . . . . .	60
5-15	Top Surface After 100 Cycles . . . . .	61
5-16	Bottom Surface After 100 Cycles . . . . .	61
5-17	Post-Test Inspection Surface Map, Run No. 100 . . . . .	62
5-18	Surface Cracks After 100 Cycles . . . . .	63
5-19	Kink in Support Rib . . . . .	64
5-20	Insulation After 100 Cycles . . . . .	65
5-21	Insulation After 100 Cycles . . . . .	65
A-1	Flatness Survey Location Map . . . . .	72

## TABLES

3-1	Weight Analysis . . . . .	25
5-1	Test Log . . . . .	57
A-1	Load Deflection Survey, Flat No. 7 . . . . .	73
A-2	Flatness Survey No. 2, After Cycle No. 10 . . . . .	73
A-3	Flatness Survey No. 3, After Cycle No. 19 . . . . .	74
A-4	Flatness Survey No. 4, After Cycle No. 40 . . . . .	74
A-5	Flatness Survey No. 5, After Cycle No. 50 . . . . .	75
A-6	Flatness Survey No. 6, After Cycle No. 60 . . . . .	75
A-7	Flatness Survey No. 7, After Cycle No. 80 . . . . .	76
A-8	Flatness Survey No. 8, After Cycle No. 100 . . . . .	76

## Section 1

### SUMMARY

The results of a thermal-structural test program to verify the performance of a metallic/radiative Thermal Protection System (TPS) under reentry conditions are presented. This TPS panel is suitable for multiple reentry, high L/D space vehicles, such as the NASA Space Shuttle, having surface temperatures up to  $1200^{\circ}\text{C}$  ( $2200^{\circ}\text{F}$ ). The TPS panel tested consists of a corrugation-stiffened, beaded-skin TD Ni-20Cr metallic heat shield backed by a flexible fibrous quartz and radiative shield insulative system. Test conditions simulated the critical heating and aerodynamic pressure environments expected during 100 repeated missions of a reentry vehicle. Temperatures were measured during each reentry cycle; heat-shield flatness surveys to measure permanent set of the metallic components were made every 10 cycles. The TPS panel, in spite of localized surface failures, performed its designated function.

## Section 2

### INTRODUCTION

The development of high-temperature metallic heat shield thermal protection systems (TPS) for reentry vehicles having high L/D characteristics has been underway at Grumman Aerospace since 1969. This development was motivated by the NASA Space Shuttle and its related technology requirements. Grumman was involved in the NASA Alternate Space Shuttle Concepts Study (NASA Contract NAS 1-1160), the results of which are presented in Ref 1, and prepared a proposal for the design and production of the Space Shuttle (Ref 2). To support these programs, a major effort to develop a reentry TPS was undertaken. This effort included development of both metallic and non-metallic heat shields covering the temperature range of 315-1370°C (600-2500°F). Metallic heat shields of titanium, Rene 41, Haynes-25, dispersion-stabilized nickel-chromium, and columbium alloys were designed and analyzed. Results of this program are presented in Ref 3, 4, and 5. A thoria-dispersion-stabilized nickel-20 percent chromium alloy (TD Ni-20Cr) metallic heat shield was developed for application in the reentry surface temperature range of 970-1200°C (1800-2200°F).

Since late 1969, Grumman has sponsored an IRAD program directed toward development of metallic TPS components for the Space Shuttle. Initially, this program investigated the development of heat shields of cobalt-based alloys such as Haynes-25 and Haynes-188. Four generations of cobalt-based alloy TPS panels were designed, fabricated, and tested under simulated launch and reentry conditions, including heating, pressure loads, and acoustic loads. All of these panels were of corrugation-stiffened, beaded skin. The results of tests on these panels and of extensive structural analysis are reported in Ref 5 through 11. During the course of this program, analytical techniques were developed specifically for a metallic TPS.

The design approach developed for the cobalt-based-alloy panels was extended to TD Ni-20Cr. Grumman designed and fabricated some small subpanels of TD Ni-20Cr which could operate in the temperature range of 970-1200°C (1800-2200°F). These panels were joined by spotwelding, and were built primarily to develop

manufacturing expertise. This experience demonstrated that the corrugation-stiffened design was feasible for the manufacture of TD Ni-20Cr TPS panels.

In late 1970, as part of the Space Shuttle European Technical Assistance Agreement, an arrangement between Avions Marcel Dassault and Grumman was made for a cooperative effort in various Space Shuttle technology areas, one of which was a high-temperature metallic TPS. Dassault, as a prime contractor for CNES (Centre National Des Etudes Spatiales), concentrated on utilization of the TD Ni-20Cr alloy and, in particular, on applying an ONERA (Organization Nationale Des Etudes de Recherches Aeronautique) developed braze process as the primary joining technique. This process offered the potential of an improved structural design because the braze did not reduce the strength of the adjacent metal. It was agreed that Dassault would apply this braze process to fabricate experimental panels using the Grumman corrugation-stiffened, beaded design.

Dassault also introduced a new thermal insulation concept to be used in conjunction with the TD Ni-20Cr structural panel. This insulation system made use of layers of an extra-low-density quartz fiber felt manufactured in France, separated by very thin reflective screens made of gold-plated micarta. This system, designated Protec-alor, was originally developed by the French firm Bronzavia for use as aircraft propulsion system thermal insulation. This insulation, although more complex, is lighter than conventional materials such as Microquartz.

Documentation of the Dassault development work leading to the TD Ni-20Cr TPS panel can be found in Ref 12, 13, and 14. The cooperative effort culminated in the fabrication by Dassault of two identical TD Ni-20Cr test panels incorporating Grumman TPS design experience with the braze and insulation experience of Dassault.

The objective of this program was to evaluate the performance of the TD Ni-20Cr panel concept under simulated reentry environments. This was to be accomplished by tests of two different panels, the first in an aerodynamic pressure/thermal environment, and the second in an acoustic/thermal environment.

An outline of this program is:

- Test the first TD Ni-20Cr TPS panel in the Grumman Environmental Test Laboratory, as follows:
  - Ten cycles of simulated entry heating with a peak surface temperature of 1200°C (2200°F)
  - Ninety cycles of a cold pressure load for ascent followed by a combined reentry heating and pressure load
  - Flatness survey of outer-panel surface after every 10 test cycles
- Deliver the second TD Ni-20Cr TPS panel to NASA Langley for testing in the thermal/acoustic facility
- Fabricate and deliver to NASA Langley attachment equipment necessary to install the panel in this facility

All measurement values contained in this report are expressed in SI and English units.

## Section 3

### PANEL CONCEPT

#### 3.1 DESIGN CRITERIA

The environment in which the TPS panel must operate was developed for the Grumman H-33 orbiter during the NASA Alternate Space Shuttle Concepts Study (Ref 1). Views of this orbiter with peak temperature isotherms are shown in Fig. 3-1. For the current study, the maximum use temperature of the TD Ni-20Cr material was arbitrarily set at  $1200^{\circ}\text{C}$  ( $2200^{\circ}\text{F}$ ). The regions where this material can be competitive are the lower forward fuselage to the rear of the nosecap, the lower outboard wing just behind the leading edge, and the lower surface of the elevon.

Trajectory parameters for the H-33 orbiter, which are reported in Ref 1, and are used to define the TPS environment used here, are shown in Fig. 3-2 through 3-5. Figures 3-2 and 3-3 define the ascent trajectory. The maximum dynamic pressure,  $29,000 \text{ N/m}^2$  (605 psf) occurs during ascent at Mach 1.25 and an altitude of 10,050 m (33,000 ft). Figure 3-4 gives vehicle reentry trajectory parameters; Fig. 3-5 gives the local surface equilibrium temperature and surface pressures for the design point 120 inches behind the nose. This point, which is noted on Fig. 3-1, was considered typical for the TD Ni-20Cr panel environment. The maximum surface temperature here is  $1200^{\circ}\text{C}$  ( $2200^{\circ}\text{F}$ ). The design conditions are taken from Ref 1, where the H-33 orbiter is defined in detail, and are:

- 100-reentry mission life
- Maximum deflection in a 51-cm (20-in.) span = 1.27 cm (0.50 in.)
- No local or overall panel flutter
- Maximum launch and boost pressures (Fig. 3-6):
  - +21,500  $\text{N/m}^2$  (+ 450 psf)\*
  - 9550  $\text{N/m}^2$  (-200 psf)

- - - - -

\*Positive pressures are normal to and toward outer panel surface; negative pressures are normal to and away from outer panel surface

- Maximum reentry pressure (Fig. 3-7):  
+2300  $\text{n/m}^2$  (+48 psf)
- Maximum reentry temperature (Fig. 3-7):  
1200°C (2200°F)

### 3.2 HEAT-SHIELD MATERIALS

In the field of metallic heat shields for Space Shuttle thermal protection systems, the dispersion-strengthened nickel-base alloys are leading candidates for the hotter heat-shield regions. These alloys are attractive because of their good high-temperature strength.

The superalloys (e.g., nickel alloy Rene 41 and cobalt alloy Haynes-25) retain high-temperature strength to about 970°C (1800°F). Above this temperature, the refractory metal alloys (e.g., columbium alloy Cb-752 or tantalum alloy T-222) have high-temperature strength but, because of their rapid oxidation in air, they require protective coatings, which, for repeated re-use, have questionable reliability.

Between the superalloys and the coated refractory metals is the class of dispersion-strengthened alloys such as TD Ni-20Cr which offer adequate high-temperature strength in air in an uncoated condition, in the temperature range of 970-1200°C (1800-2200°F).

Under DOD- and NASA-sponsored programs (Ref 15 through 19), a number of dispersion-strengthened alloys have been developed primarily for turbojet engines and appear useful for Space Shuttle heat shields. In all of these studies it has been determined that the high-temperature strength is associated with the dispersion of very small particles of metal oxide - one to four percent by volume - in a metal matrix. The dispersoid, thorium dioxide ( $\text{ThO}_2$ ), has been used mainly because of its good chemical stability.

Most of these alloys are produced from powders. However, the method of compacting the powders, the blending and making of the alloy, along with the sheet-rolling processes, varies from one manufacturer to another. As a result, alloys with identical composition can have appreciably different properties, depending on the manufacturer.

Of all the dispersion-strengthened alloys, TD Ni-20Cr is the most developed for heat-shield applications because it offers the best combination of strength, oxidation resistance, and availability. This alloy was originally developed by E.I. DuPont deNemours, Inc., and the rights and facilities to produce it sold subsequently to Fansteel, Inc.

The TD Ni-20Cr supplied to Grumman/Dassault by NASA for fabricating the TPS panels in this program were manufactured by Fansteel, Inc., under the NASA dispersion-strengthened alloy development program. This alloy has a nominal composition of Ni, 20% Cr, and 2%  $\text{ThO}_2$ . The mechanical and physical properties are listed in Ref 5. The nominal material thicknesses were 0.025 cm (0.010 in.) for the sheets used in fabricating the basic heat shield and 1.25 cm (0.5 in.) for rods used in fabricating fasteners, etc. The material was easy to fabricate into the heat-shield configurations used in this study and required no additional preparation other than that used in other similar Grumman heat-shield programs employing superalloys. The only exception was in the braze process used by Dassault to attach the outer beaded skin to the corrugation.

The insulation materials and design concept are discussed in a following section.

### 3.3 CONFIGURATION

The Dassault TD Ni-20Cr TPS test article is the intersection of four 50.8- by 101.6-cm (20- by 40-in.) reradiative skin panels supported on 13.97-cm (5.5-in.) support rib standoffs located on a 50.8-cm (20-in.) pitch.

A photograph of the assembled test article is shown in Fig. 3-8. It shows the metallic frontface, an aluminum backface plate, metallic standoff supports, and a two-layer insulation system sandwiched between these components. The coils of wire shown are instrumentation leads. A design concept drawing is presented in Fig. 3-9.

The test article represents the intersection of four 50.8-cm (20-in.) square heat-shield panels. A longitudinal expansion joint and a lateral panel splice are incorporated to verify feasibility of these design features. Each panel consists of a beaded 0.025-cm (0.010-in.) corrugation. These two formed sheets are joined along

the flats between beads by a French-developed proprietary brazing process. The combined beads and corrugations form a panel with high longitudinal bending stiffness having good flutter characteristics and which transfers aerodynamic pressure loads to the support rib standoffs by simple beam action.

Thermal expansion in the lateral direction (perpendicular to the beads) is permitted by flexing of the beads, eliminating the need for lateral expansion joints. A longitudinal expansion joint is located at 101.6 cm (40-in.) intervals or at every other support rib standoff to "absorb" the thermal expansion from 101.6 cm (40 in.) of panel or two 50.8-cm (20-in.) simply supported spans. (Details of the joint design can be seen in Fig. 3-10.) The support ribs at this joint are designed to flex as the skins expand, yet remain rigid enough to transfer panel loads vertically to the vehicle primary structure. Between the expansion joints are fixed supports, designed to transfer panel loads without flexing. On the test article, the fixed supports are located at the ends of the panels; their details can be seen in Fig. 3-8. These fixed supports have brackets placed at 19.05-cm (7.5-in.) intervals, which are designed to take all longitudinal drag loads.

Each support rib consists of a 0.025-cm (0.010-in.) beaded web mechanically fastened to the frontface skins above and to the aluminum structure below with angle clips located at each flat between the beads. The web beads are of constant cross-section and are designed to relieve thermal stress between the hot skin panel and the cool primary structure. A splice parallel to the beads is located along the middle flat of the panel. Here, joining is accomplished by a row of threaded TD Ni-20Cr fasteners spaced 5.08 cm (2 in.) apart. All parts are made of TD Ni-20Cr and are joined with TD Ni-20Cr threaded fasteners.

### 3.4 UNIT WEIGHT

The TD Ni-20Cr TPS panel weight was calculated (Table 3-1) and measured in the laboratory. The calculated weight, 7.86 kg (17.3 lb) is slightly less than the measured 8.59 kg (18.9 lb) due to the instrumentation still attached to the panel. The calculated total unit weight is then  $15.14 \text{ kg/m}^2$  (3.09 psf) of panel, which includes  $6.71 \text{ kg/m}^2$  (1.37 psf) for the insulation package. The aluminum backface panel representing substructure is not included in these weights.

### 3.5 INSULATION CONCEPTS

The insulation assembly used in the test panel is a composite of two layers: 4.0 cm (1.57 in.) of a fibrous alumina-silica-chromia felt called Dynaflex, and 7.0 cm (2.75 in.) of Protecalor. The insulation assembly is "trapped" in place between the TD Ni-20Cr skin panels, support ribs, and aluminum heat-sink structure, obviating mechanical attachments.

Dynaflex, manufactured by the Johns-Manville Company, has a density of  $96 \text{ kg/m}^3$  (6.0 pcf), and was selected for use in the temperature range of  $900\text{--}1200^\circ\text{C}$  ( $1650\text{--}2200^\circ\text{F}$ ). Because there was no TD Ni-20Cr foil available that could be used for bagging needed to prevent moisture absorption by the insulation, the layer was inserted without a metal foil case. The second layer of insulation is the Protecalor. This system consists of a series of very thin reflective screens separated by layers of lightweight quartz wool called Astroquartz. For the temperature range of  $600\text{--}900^\circ\text{C}$  ( $1100\text{--}1650^\circ\text{F}$ ), the reflective screens are gold-plated micarta  $20 \mu\text{m}$  (0.0008 in.) thick. From  $400\text{--}600^\circ\text{C}$  ( $750\text{--}1100^\circ\text{F}$ ), the reflective screens are aluminum  $20 \mu\text{m}$  (0.0008 in.) thick. The Astroquartz, which is made by the French company Quartz et Silice, is made of fibers drawn from pure silica and has a density of  $16 \text{ kg/m}^3$  (1.0 pcf). The total density of the Protecalor is  $21 \text{ kg/m}^3$  (1.31 pcf), making it an extremely lightweight insulation system. The high thermal efficiency of this insulation system is seen by comparing its specific conductivity ( $k\rho$  - product) to that of Microquartz and Dynaquartz, as shown in Fig. 3-11.

The entire Protecalor system is enclosed in a protective bag that improves handling and prevents excessive moisture absorption. This bag has a top and sides made of  $76 \mu\text{m}$  (0.003 in.) Inconel foil. The bottom of the bag is made of 10.0-mm (0.40-in.) polyimide foam, weighing  $48 \text{ kg/m}^3$  (3.0 pcf) and having an upper temperature limit of  $400^\circ\text{C}$  ( $750^\circ\text{F}$ ). The polyimide foam serves to rigidize the insulation package, is moistureproof, and is also an effective insulation. The insulation system and temperature range are shown in Fig. 3-12 and the detailed unit weight breakdown is shown in Table 3-1.

### 3.6 FABRICATION & JOINING CONCEPTS

The TD Ni-20Cr external skin structure is fabricated by cold break-forming of beads and corrugations in 0.025-cm (0.010-in.) sheet material, and then brazing them together along the flats between the beads with a proprietary brazing process. This braze process, developed by ONERA, was studied extensively by Dassault prior to fabricating this test article to determine its feasibility. Test coupons of both parent metal and brazed samples were made and tested. The test results, (Ref 14) indicate that the brazing process produces about a 10% loss of strength to the material. This is far superior to other joining techniques previously used with the material. Although the test results show a marked increase in creep at high temperature, there is no impact on this design due to creep because the panel was not creep-critical.

Threaded fasteners made of TD Ni-20Cr were machined from rod stock and were used to join the beaded, corrugation-stiffened skins to the support ribs and to join the skins along longitudinal splices. These fasteners consist of screws and nuts.

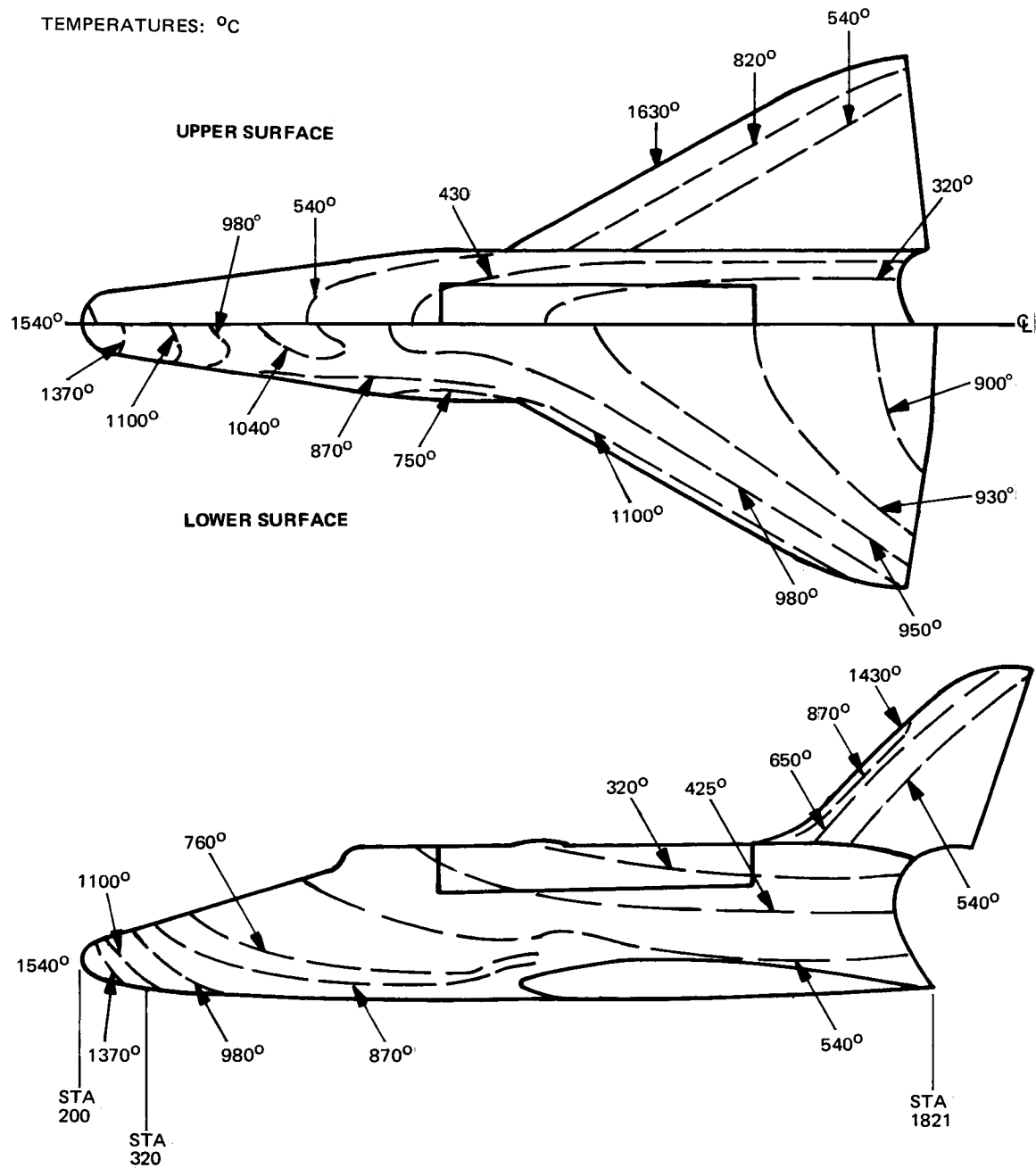


Fig. 3-1 Grumman H-33 Orbiter Isotherms

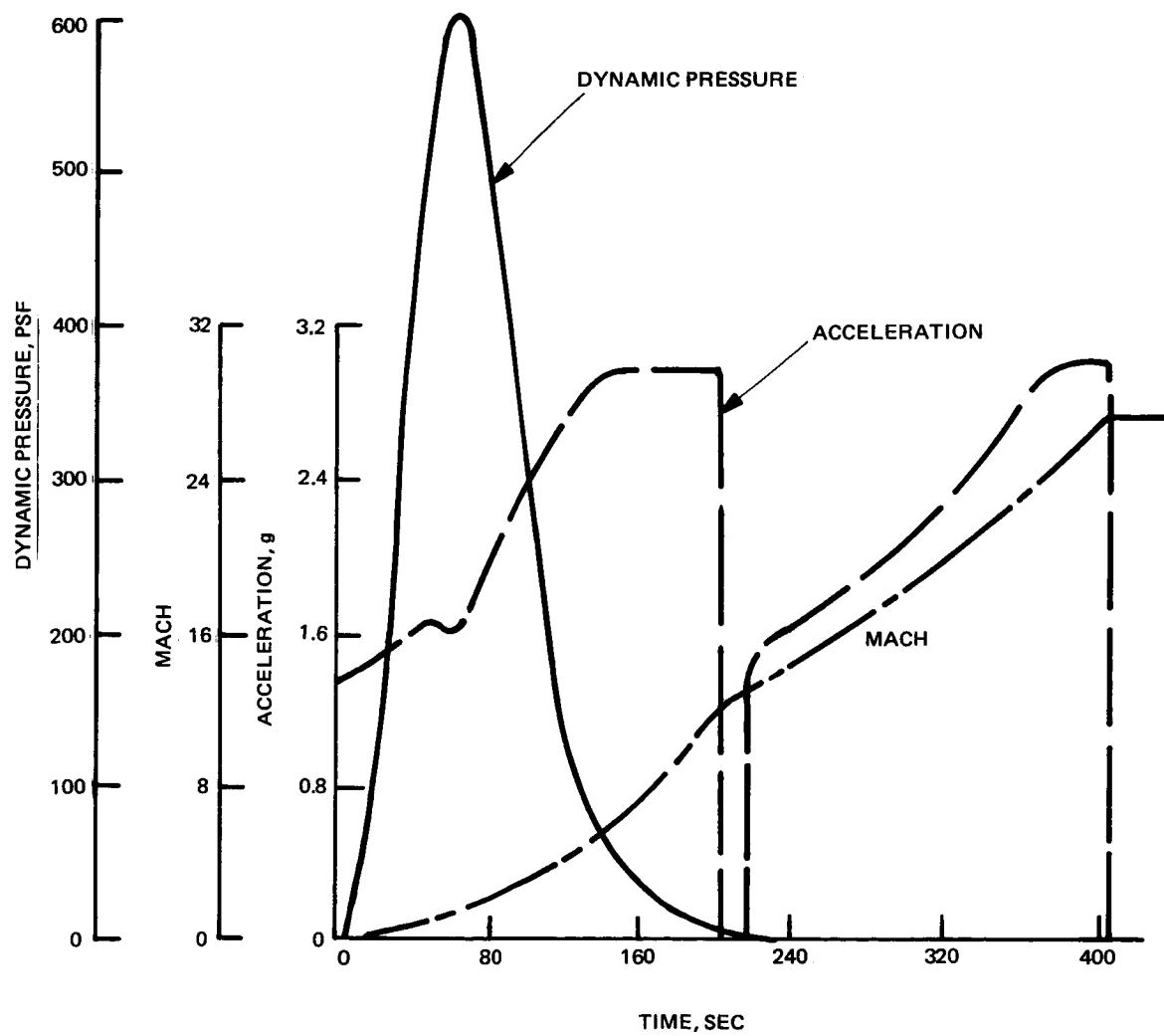


Fig. 3-2 Ascent Trajectory Parameters

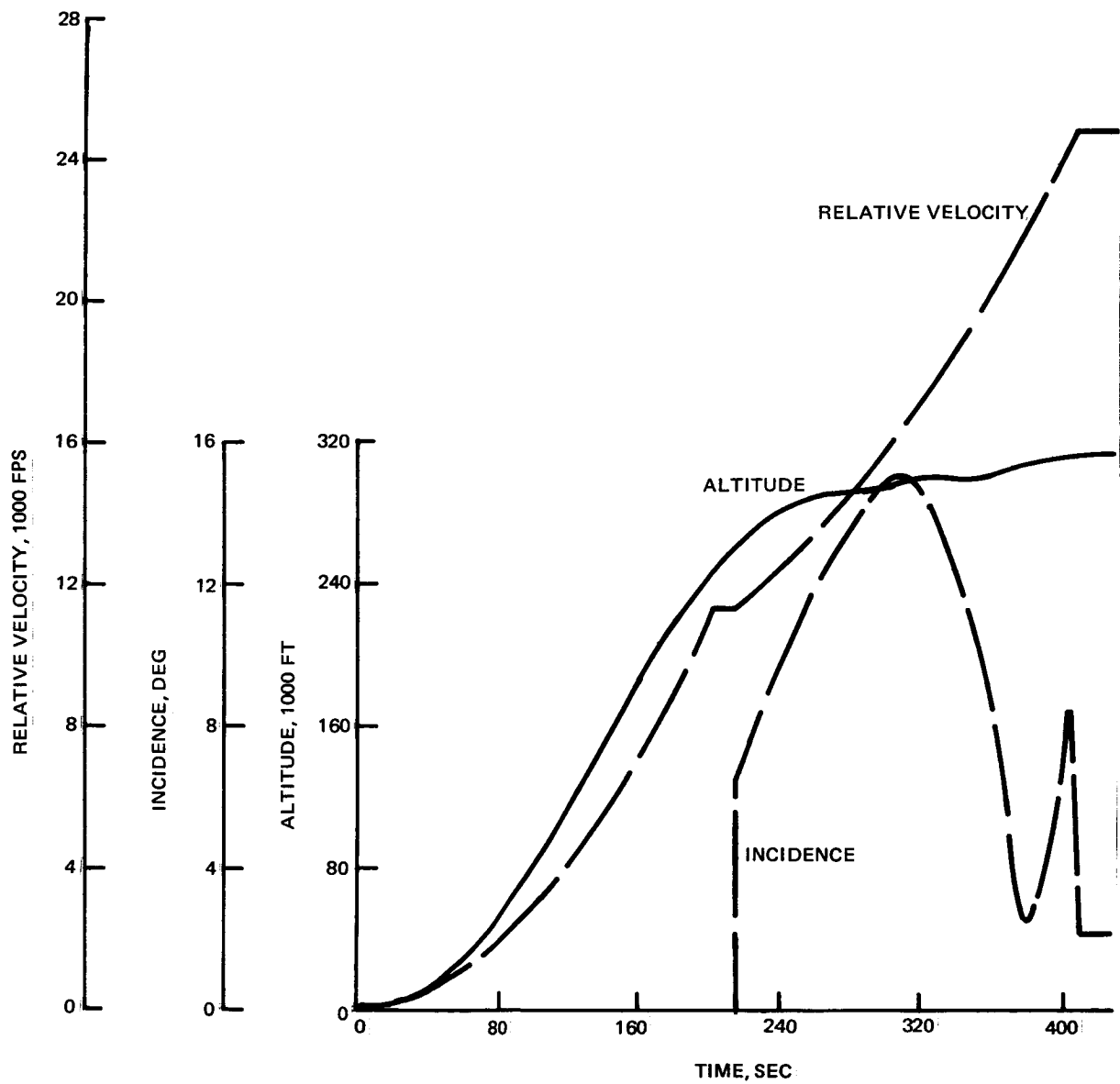


Fig. 3-3 Ascent Trajectory Parameters

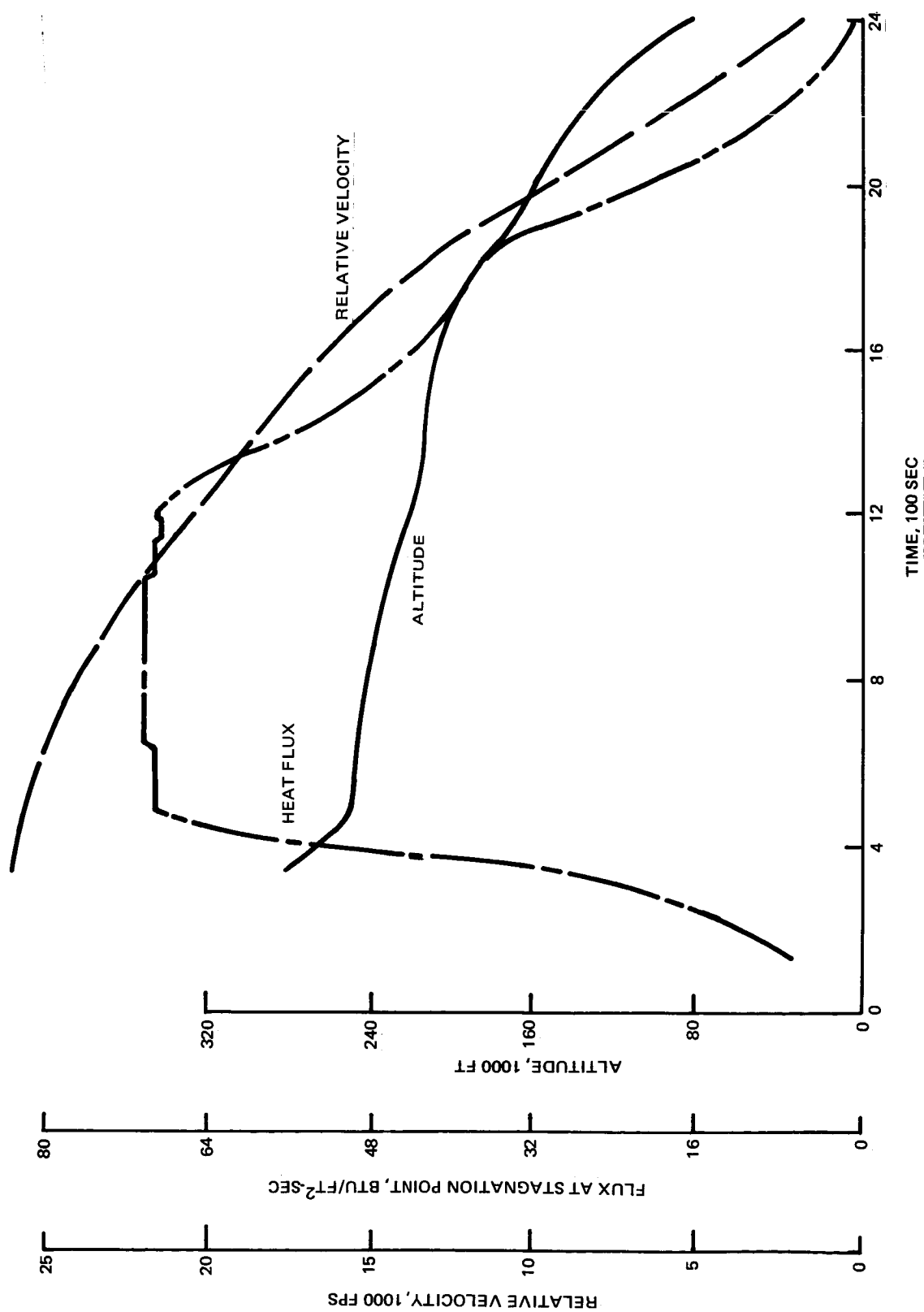


Fig. 3-4 Reentry Trajectory Parameters

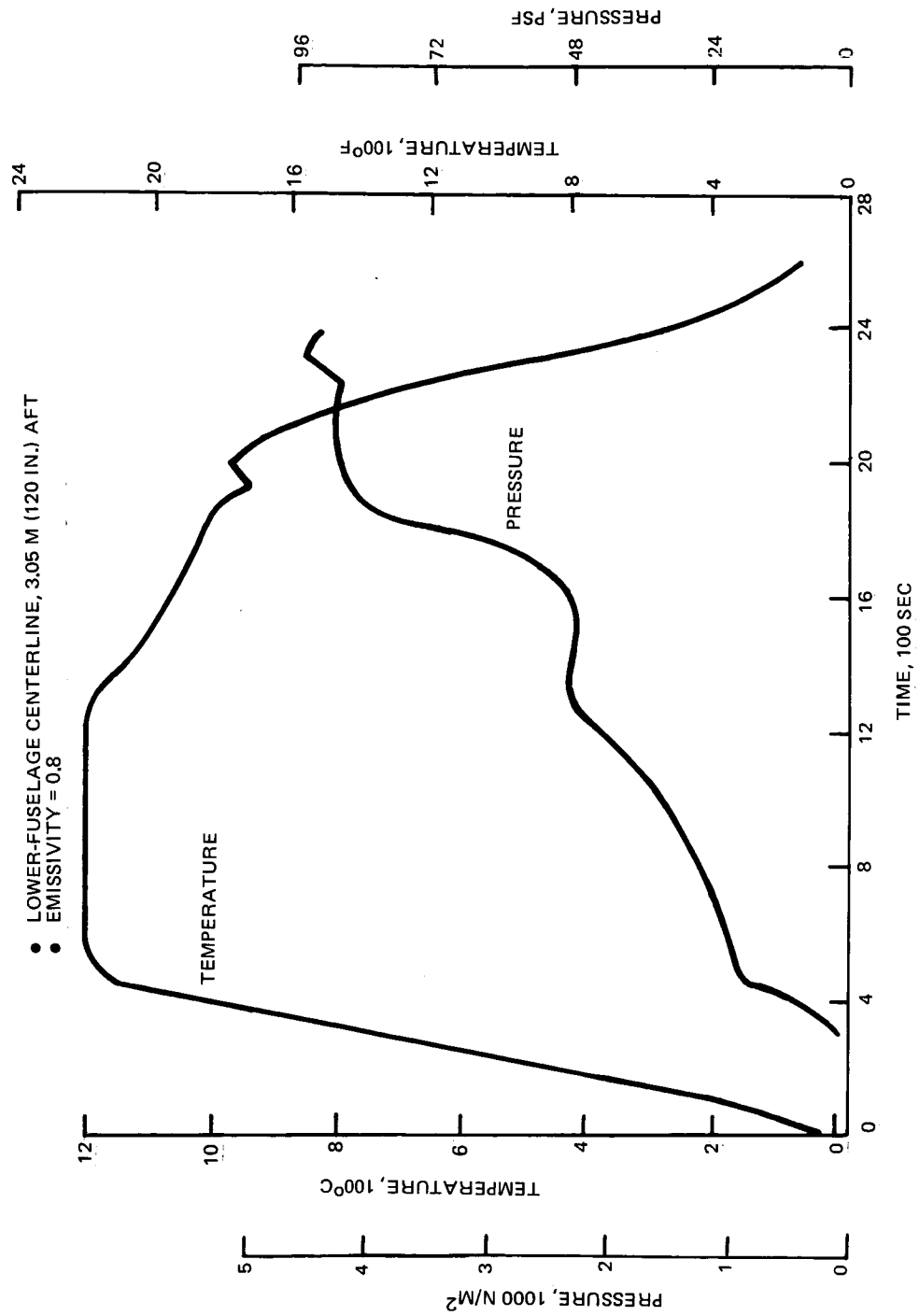


Fig. 3-5 Reentry Pressure & Temperature

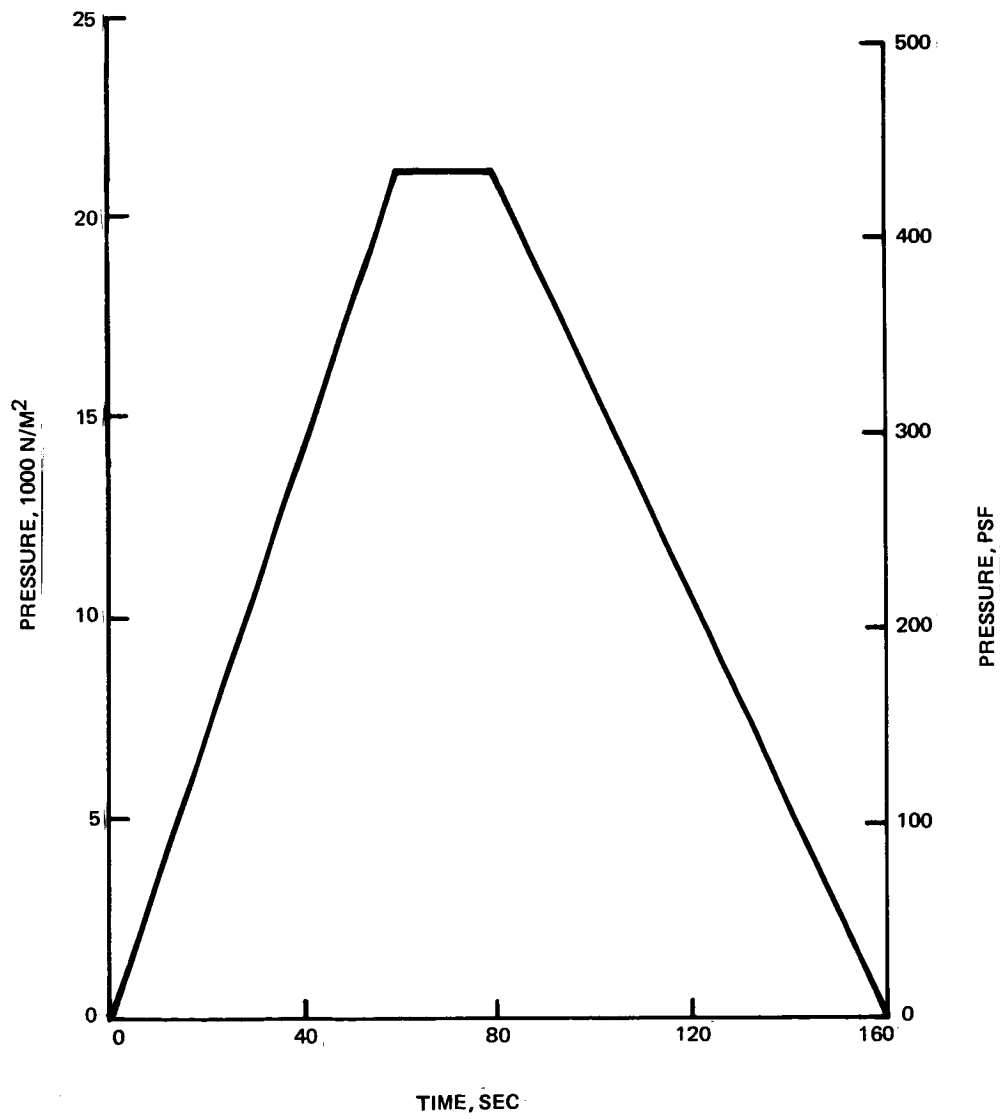


Fig. 3-6 Ascent Pressure Test Condition

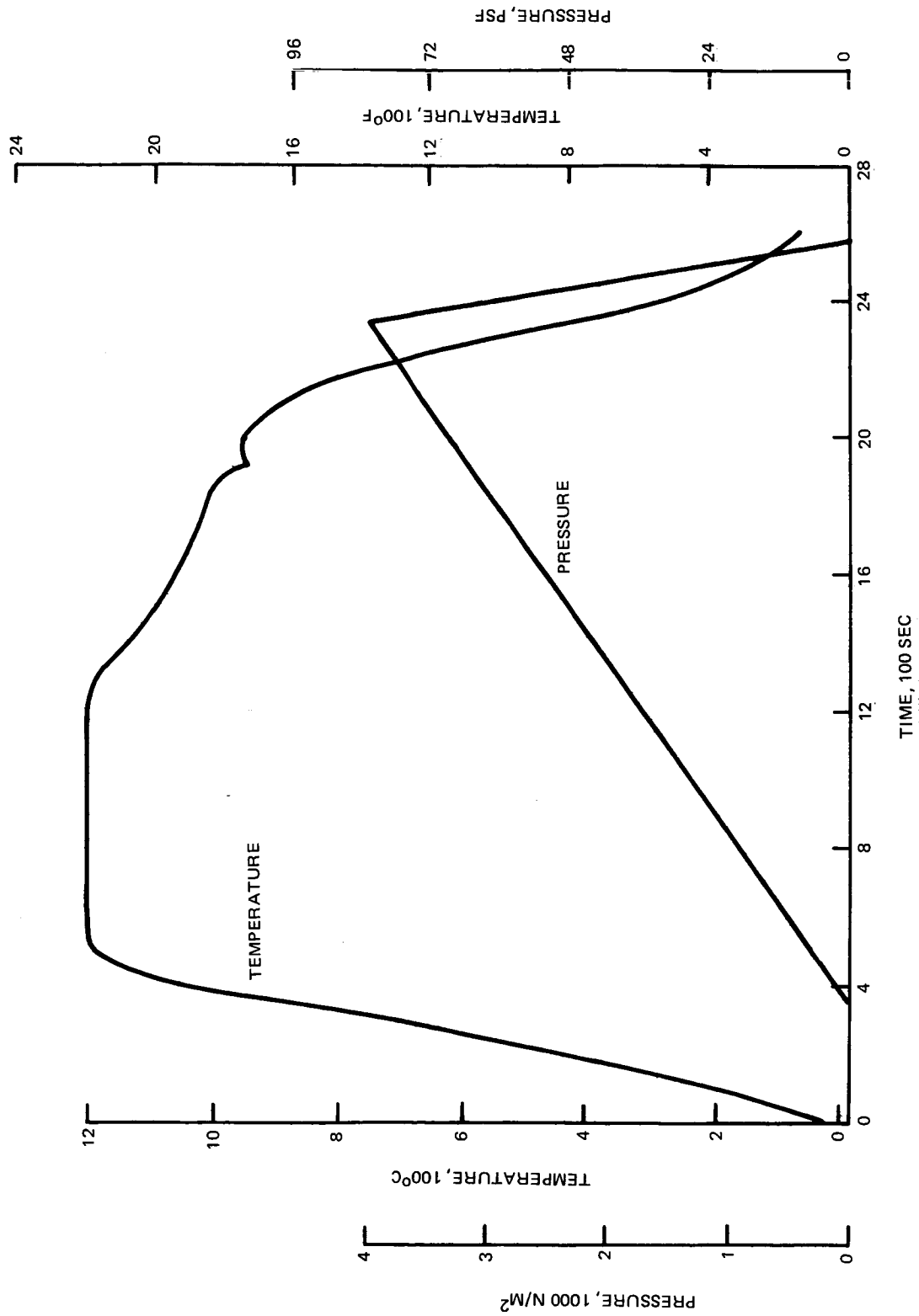


Fig. 3-7 Reentry Pressure & Temperature Test Conditions

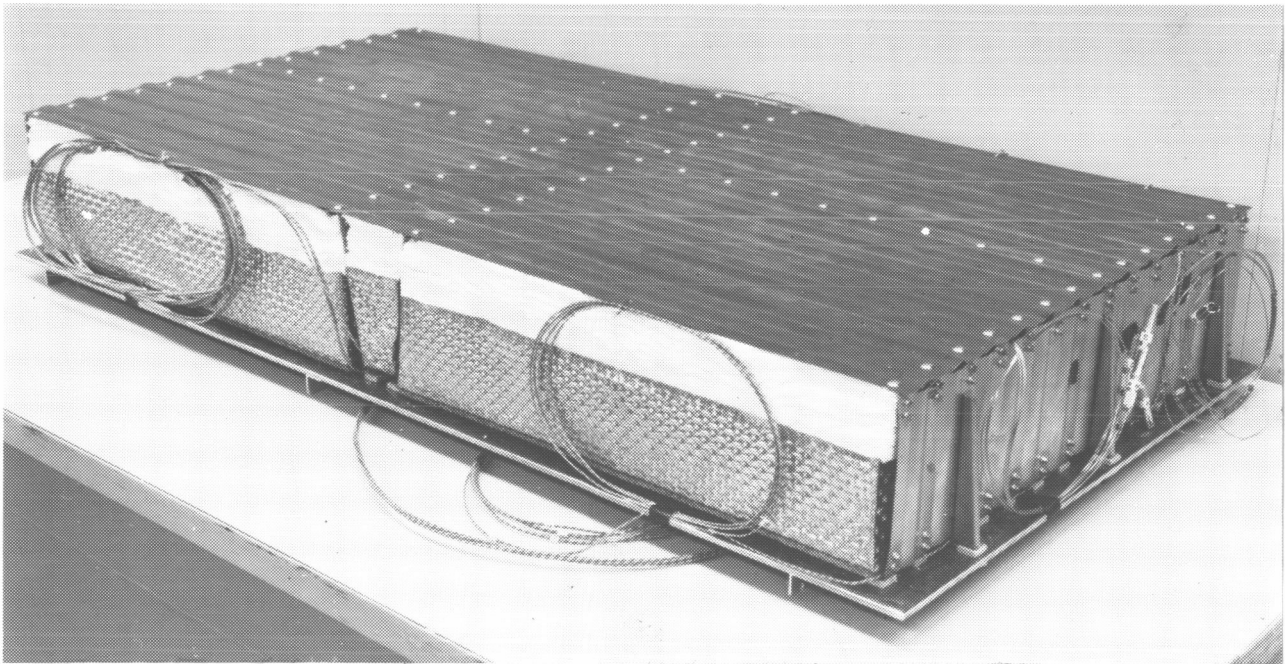


Fig. 3-8 Test Article

(BLANK)

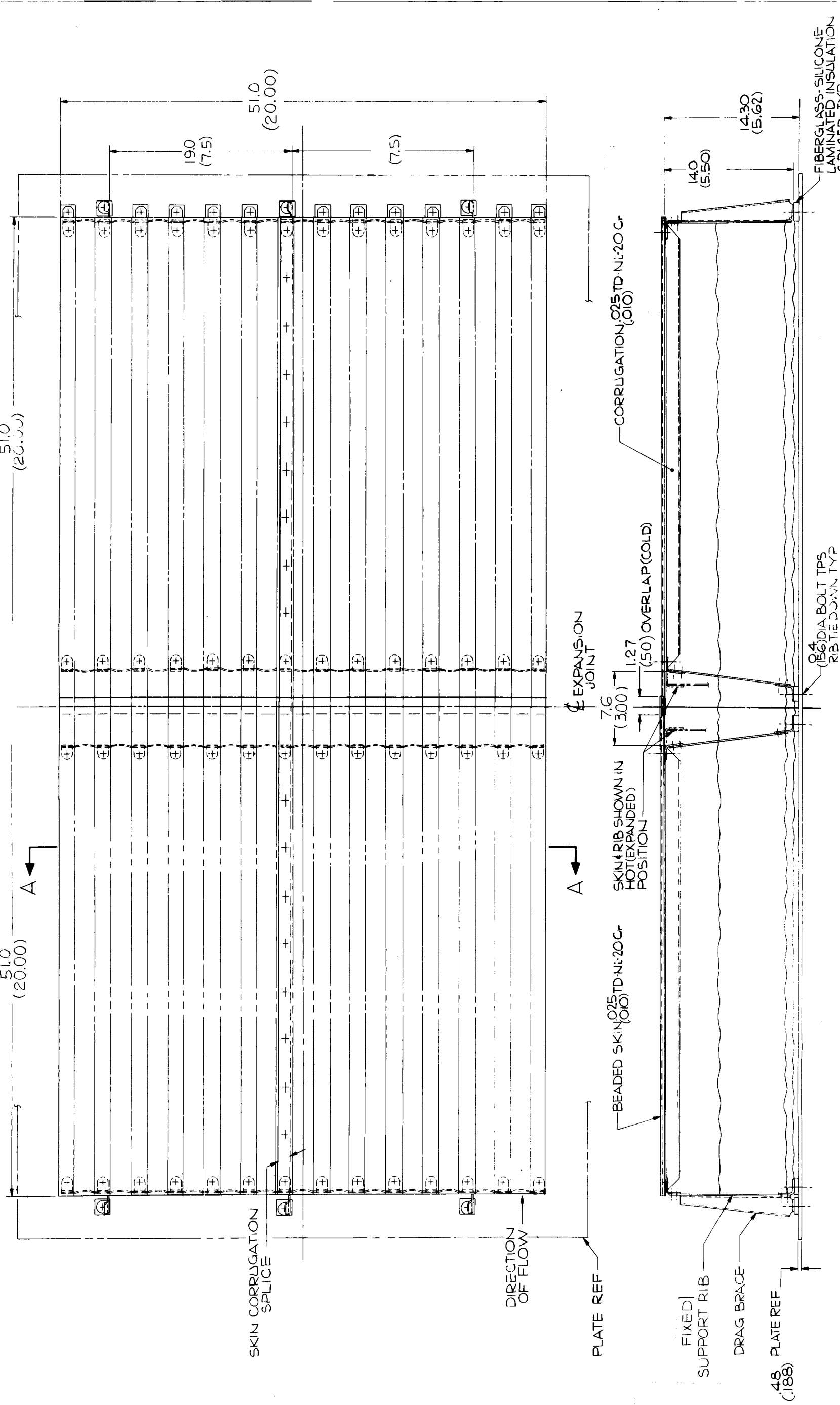
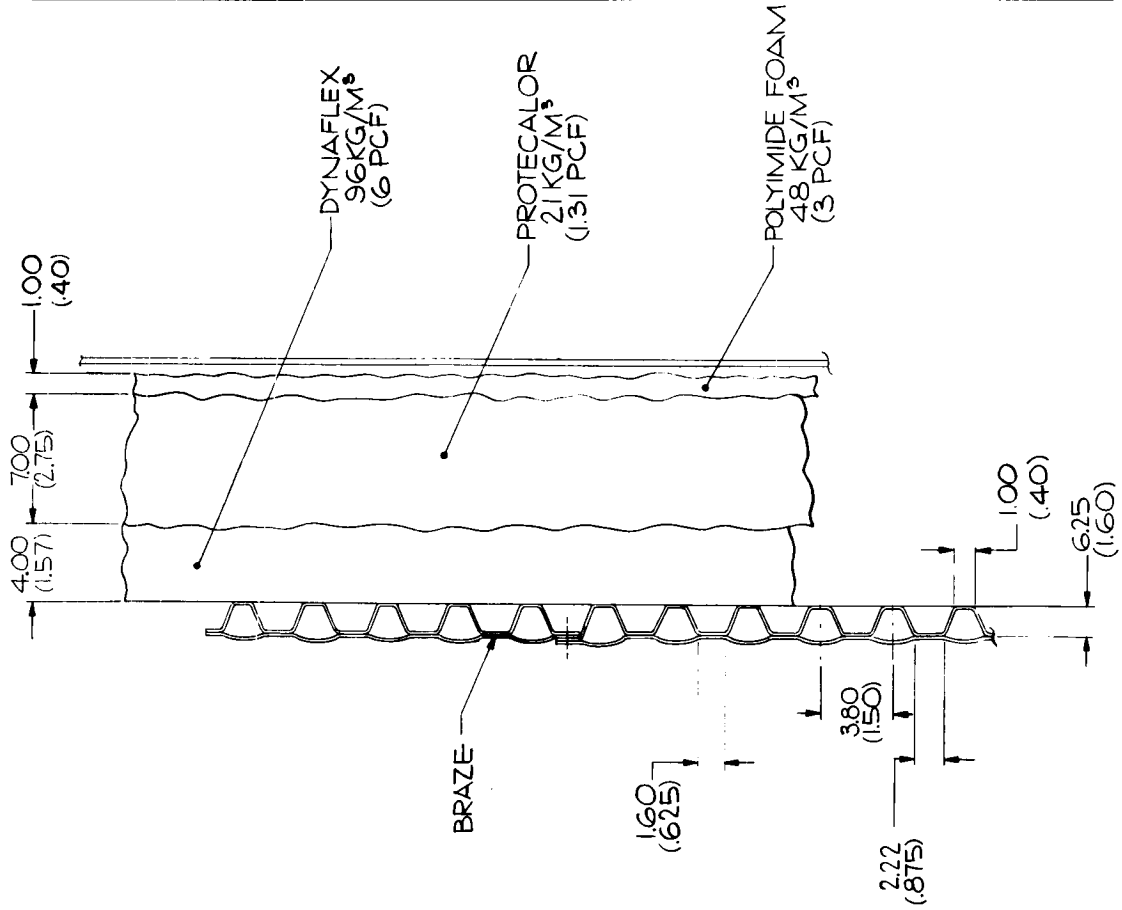
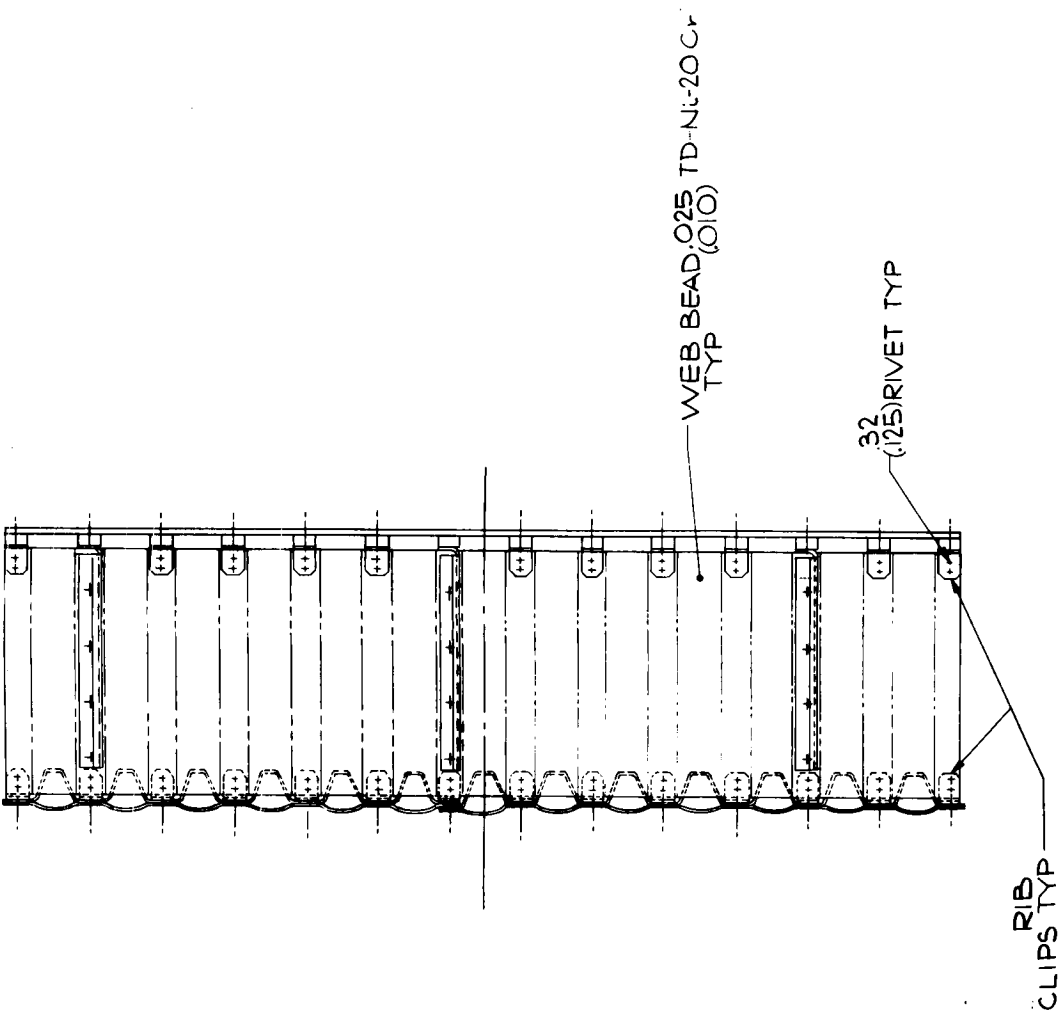




Fig. 3-10 Expansion Joint Detail



SECTION A-A

NOTE: DIMENSIONS ARE IN CENTIMETERS (INCHES)

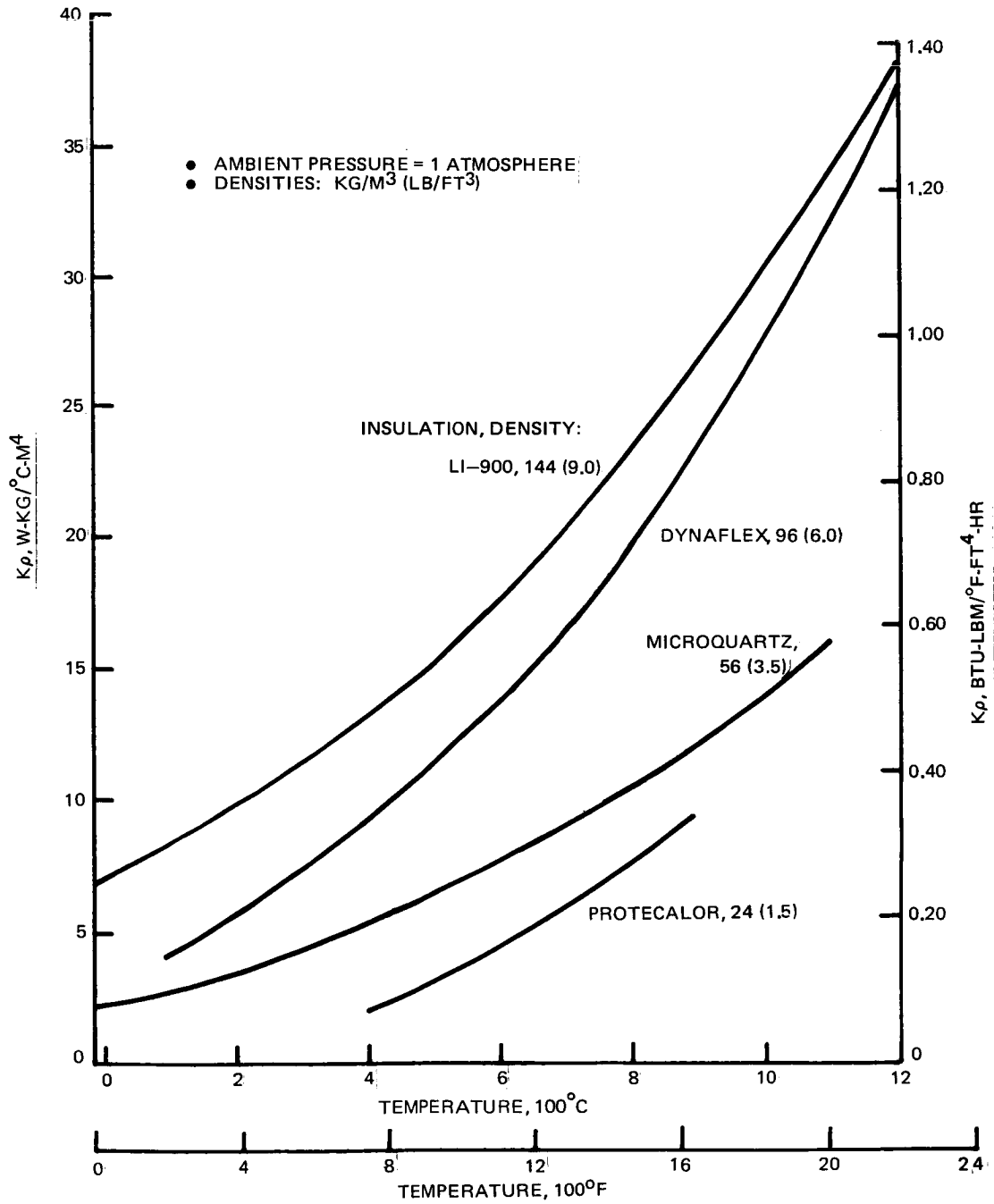
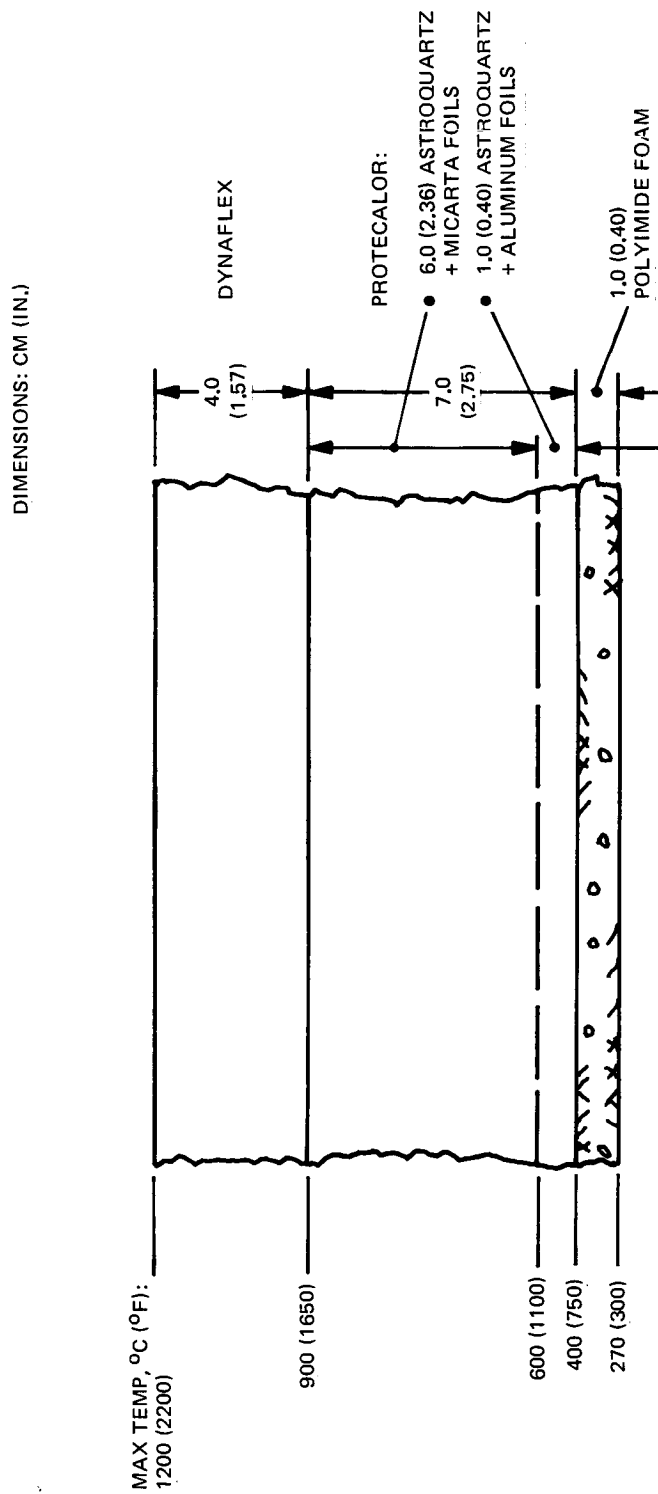


Fig. 3-11 Insulation Specific Conductivity



DENSITY, KG/M<sup>3</sup>(LB/FT<sup>3</sup>):

- DYNAFLEX, 96 (6)
- PROTECALOR, 21 (1.31)
- POLYIMIDE FOAM, 48 (3)

Fig. 3-12 Panel Insulation System

Table 3-1 Weight Analysis

	Length		Width		Thickness		Volume		Density		Weight		Area		Unit Weight	
	cm	in.	cm	in.	cm	in.	cm <sup>3</sup>	in. <sup>3</sup>	kg/m <sup>3</sup>	lb/in. <sup>3</sup>	kg	lb	m <sup>2</sup>	ft <sup>2</sup>	kg/m <sup>2</sup>	lb/ft <sup>2</sup>
BARE PANEL																
Beaded Skin	102	40	50.8	20	0.025	0.01	131	8.0	8590	0.31	1.12	2.48	0.52	5.6	2.17	0.443
Corrugation	91	35.8	81.3	32	0.025	0.01	188	11.45	8590	0.31	1.61	3.55	0.52	5.6	3.11	0.634
End Rib Web	26.4	10.4	50.8	20	0.025	0.01	34.1	2.08	8590	0.31	0.295	0.65	0.52	5.6	0.568	0.116
Center Support Rib	13.2	5.2	50.8	20	0.025	0.01	17.1	1.04	8590	0.31	0.145	0.32	0.52	5.6	0.28	0.057
Web Clips	92.5	36.4	0.612	0.24	0.025	0.01	14.35	0.875	8590	0.31	0.122	0.27	0.52	5.6	0.235	0.048
Drag Support	6.36	2.5	13.7	5.4	0.025	0.01	2.21	0.135	8590	0.31	0.018	0.04	0.52	5.6	0.0353	0.007
Fiberglass Spacer	11.94	4.7	50.8	20	0.305	0.12	185	11.28	1940	0.07	0.358	0.79	0.52	5.6	0.69	0.141
Hardware & Misc											0.68	1.50	0.52	5.6	1.31	0.268
Subtotal											4.35	9.60			8.4	1.714
INSULATION																
Dynaflex	102	40	50.8	20	4.0	1.57	20,600	1255	96.2	0.00347	2.0	4.4	0.52	5.6	3.84	0.785
Protecalor	102	40	50.8	20	6.52	2.75	36,100	2200	21	0.000758	0.762	1.68	0.52	5.6	1.47	0.3
Polyimide	102	40	50.8	20	1.02	0.4	5250	320	48	0.001735	0.254	0.56	0.52	5.6	0.489	0.1
Bag (Top & Sides)	64.8	25.5	115.5	45.5	0.00763	0.003	55.6*	3.39*	8500	0.307	0.472	1.04	0.52	5.6	0.915	0.187
Subtotal											3.48	7.68			6.73	1.372
Total											7.83	17.28			15.1	3.086
*Subtract four corner squares, 7 cm (2.75 in.) each; A= 7300 cm <sup>2</sup> (1130 in. <sup>2</sup> )																

## Section 4

### TEST APPARATUS & PROCEDURES

#### 4.1 HEATING & LOADING EQUIPMENT

The test setup used for the thermal-structural testing of the TPS panel is shown in Fig. 4-1 and a schematic of the control system is shown in Fig. 4-2. Heat is provided by a 71- by 102-cm (28- by 40-in.) array having 30 1.9-cm (3/4-in.) diameter by 71-cm (28-in.) long silicon carbide radiant-heating elements. In this configuration, the array can draw 400 amperes at 400 volts, easily producing the required 1200°C (2200° F) peak temperature over the surface of the test article and also the required transient frontface temperature.

The heating array is powered and controlled by a power-control unit (THERMAC). Control is automated through a data tracker system which takes inputs from thermocouples on the panel frontface and regulates power to provide the programmed time-temperature history. The average of two frontface thermocouple outputs provides the input to the data tracker.

Mechanical loads simulating aerodynamic pressures are applied to the specimen by an array of loading wires attached at 84 discrete points on the specimen frontface. (The loading system is detailed in Fig. 4-3.) These 0.11-cm (0.046-in.) diameter loading wires penetrate the insulation blanket and backface aluminum heat sink to a whiffle-tree apparatus that combines two load wires into one load link, and repeats this process through seven levels to a single load point. This point is at the center of a beam having a pneumatic actuator at one end, which provides programmed reentry loads, and a manually operated hydraulic actuator at the other end, which inputs the room-temperature ascent pressure loads. A calibrated load cell at the single load point in the center of the beam provides load feedback to a programmed servoactuator, which operates the pneumatic actuator.

The loading wires are attached to 1.27-cm (0.5-in.) diameter washers, which transmit the loads to the TD Ni-20Cr frontface structure. Both loading wires and washers are made of Haynes-25 cobalt-base alloy. Because of the linkage arrangement,

the whiffle tree can accommodate a number of wire failures. However, in the event one of the loading wires fails, its load is transferred to the adjacent loading wire, which now carries both loads. This causes a higher local load and some minor adjustments in the whiffle-tree linkage levels, but does not change the total load carried in the panel.

A diagram showing the loading wire locations on the test article frontface is presented in Fig. 4-4. The load wires are joined along the lettered rows in the upper levels of the whiffle-tree. This means that if a loading wire in Row A fails, its load will be transferred to the adjacent loading wire in Row A. Hence, the load for a lettered row will be constant until all the loading wires in that row fail. Then the load for the row will be transferred to an adjacent row.

#### 4.2 INSTRUMENTATION

The metallic panel is instrumented with 25 chromel/alumel thermocouples, as shown in Fig. 4-5. Of these, five act as surface control transducers, five provide surface measurements, and the remainder measure support rib, corrugation, and aluminum heat-sink temperatures at various locations. In addition, there are 16 thermocouples embedded in the insulation blanket at various depths, furnishing temperature gradients throughout the test. Temperature values were printed on two Bristol 24-point recorders and a Bristol four-pen continuous recorder.

Load data were obtained by reading the output of the calibrated load cell at discrete intervals. Readings were normally taken every 2 minutes, although during the first eight load cycles this interval was reduced to one minute.

Flatness surveys were made periodically to measure the permanent deformation in the TD Ni-20Cr structure. These surveys were accomplished with the use of a measuring bridge having seven dial indicator gages, as shown in Fig. 4-6. The measuring bridge was placed on the specimen so that the dial indicator probes touched a flat running between two beads on the metallic facesheet. The dial indicators read the elevation of the points in the flat relative to some reference elevation. In this case, the reference elevation was taken to be the dial indicator readings prior to any thermal cycling. The permanent deflection of the TD Ni-20Cr structural

panel after a temperature-load cycle was determined by taking the difference of the current dial indicator readings and the readings prior to the temperature cycling.

#### 4.3 PROCEDURES & TEST SEQUENCES

Figure 3-6 shows the transient pressure for the ascent simulation, which was applied when the panel was at room temperature or less than 38°C (100°F). Figure 3-7 shows the reentry simulation temperatures and pressures which were applied simultaneously.

The schedule of testing the TPS panel was:

1. Flatness survey
2. Ten cycles of reentry heat flux
  - a. Reentry frontface temperature profile is applied (Fig. 3-7)
  - b. Test article is cooled to less than 38°C (100°F) before next cycle is applied
3. Flatness survey
4. Ninety cycles (numbered 11 through 100) of combined reentry heat flux and static pressure load
  - a. Static ascent simulation profile, applied at room temperature (Fig. 3-6)
  - b. Reentry frontface temperature profile and programmed reentry pressure profile (Fig. 3-7) applied simultaneously
  - c. Test article is cooled to less than 38°C (100°F) before next cycle is applied
5. Flatness surveys conducted after cycle No. 19, 40, 50, 60, 80, and 100.

The first 10 cycles, which consisted of reentry heating profiles only, were intended to serve as a checkout of the test rig and a time to determine the thermal performance of the insulation blanket. When it was demonstrated, at the end of the tenth cycle, that both the test rig and insulation were performing satisfactorily, the

loading wires were installed and the combined load and temperature cycles were stored.

During cycle No. 11, the first cycle with the loading wires in place, temperature response of the backface heat sink was monitored closely to ensure that conduction through the loading wires and the degrading effect of the penetrations in the insulation would not cause a large change in the temperature response of the backface heat sink. The load wires were also monitored closely. If an excessive number, such as an entire row, failed, the loading was terminated. This procedure was followed in an attempt to prevent the local concentrated stresses at the remaining load points from becoming excessive. However, load transfer due to wire failure may have affected frontface cracking, which is described subsequently.

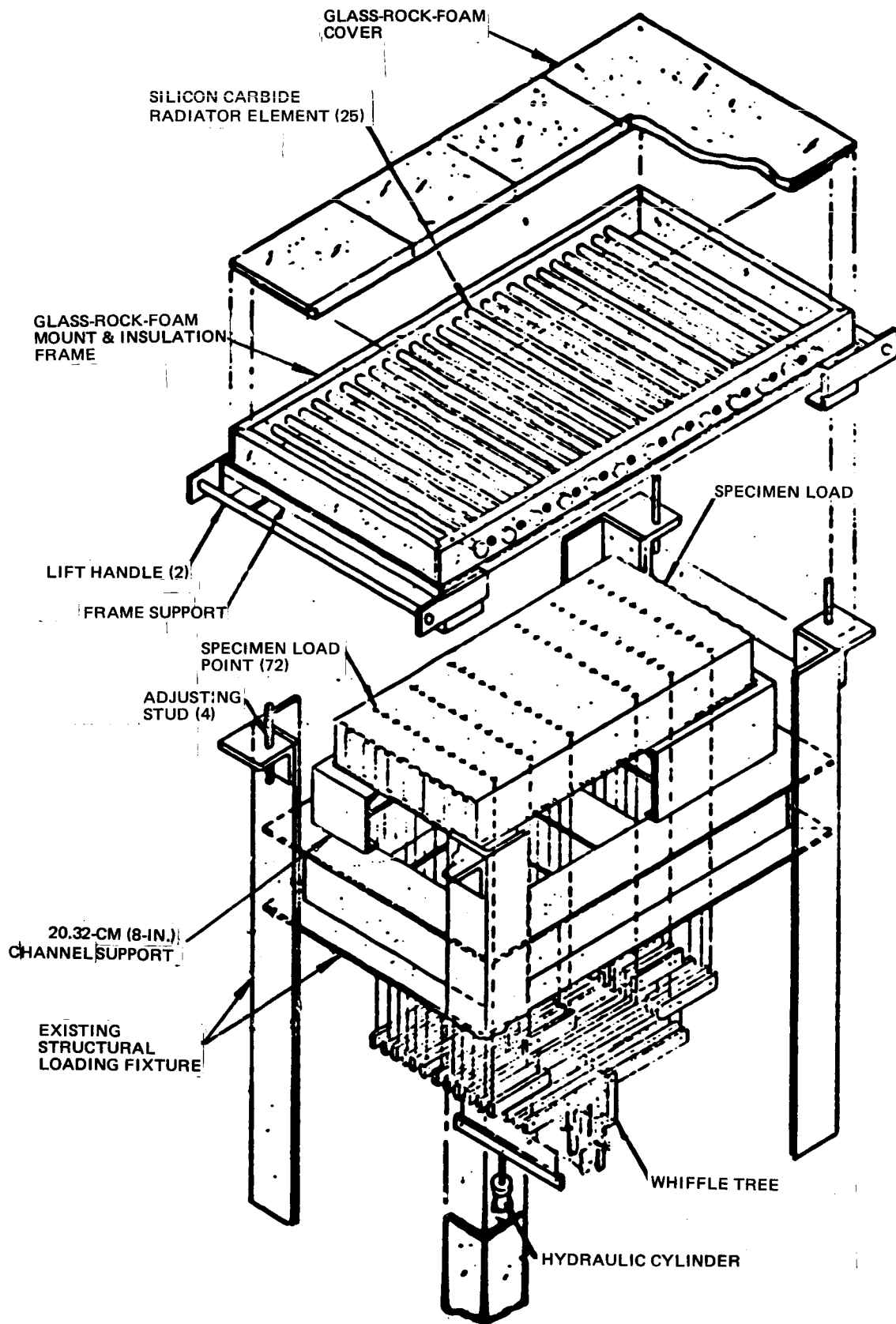


Fig. 4-1 Thermal-Structural Test Facility

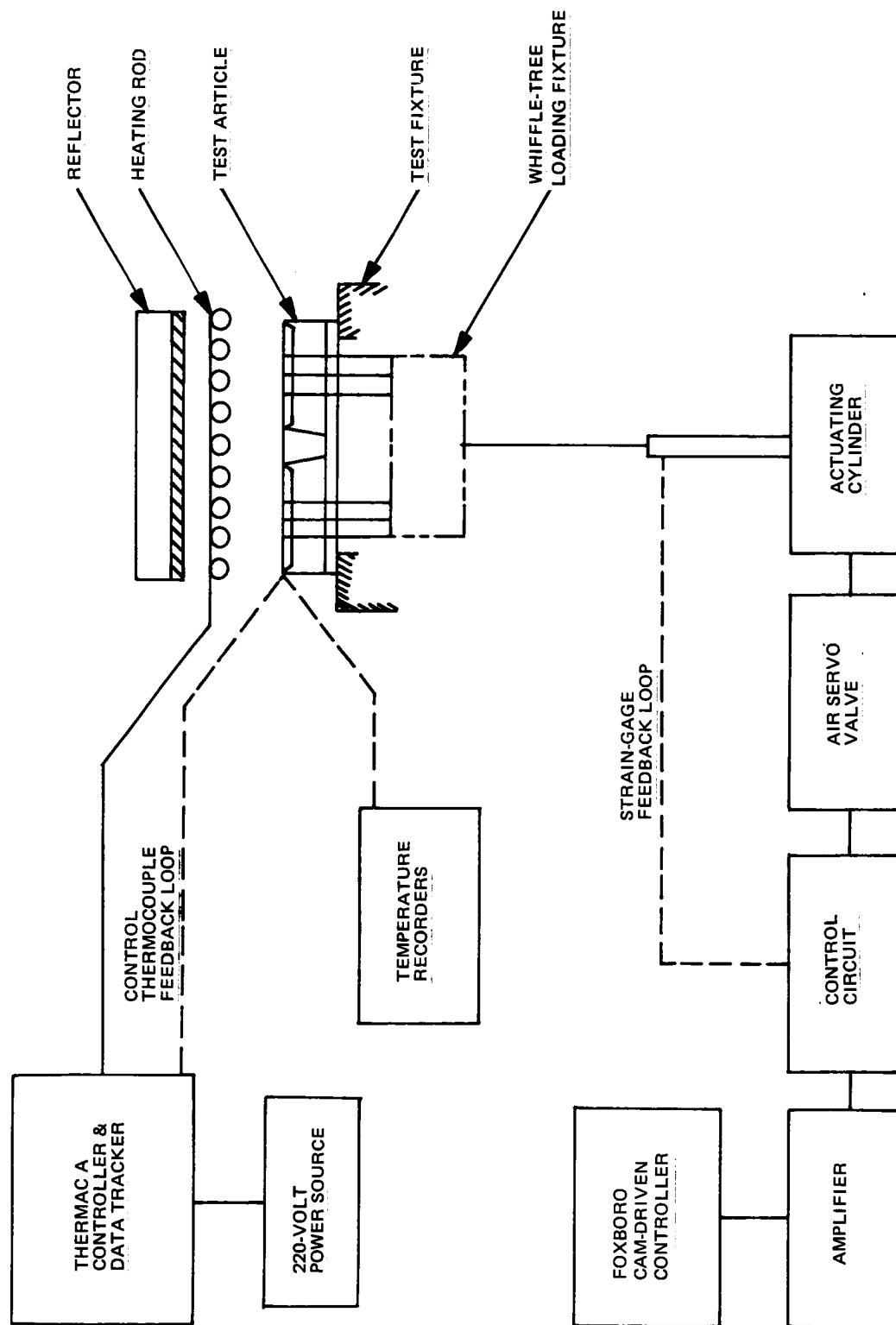


Fig. 4-2 Thermal-Structural Test Facility Control Systems

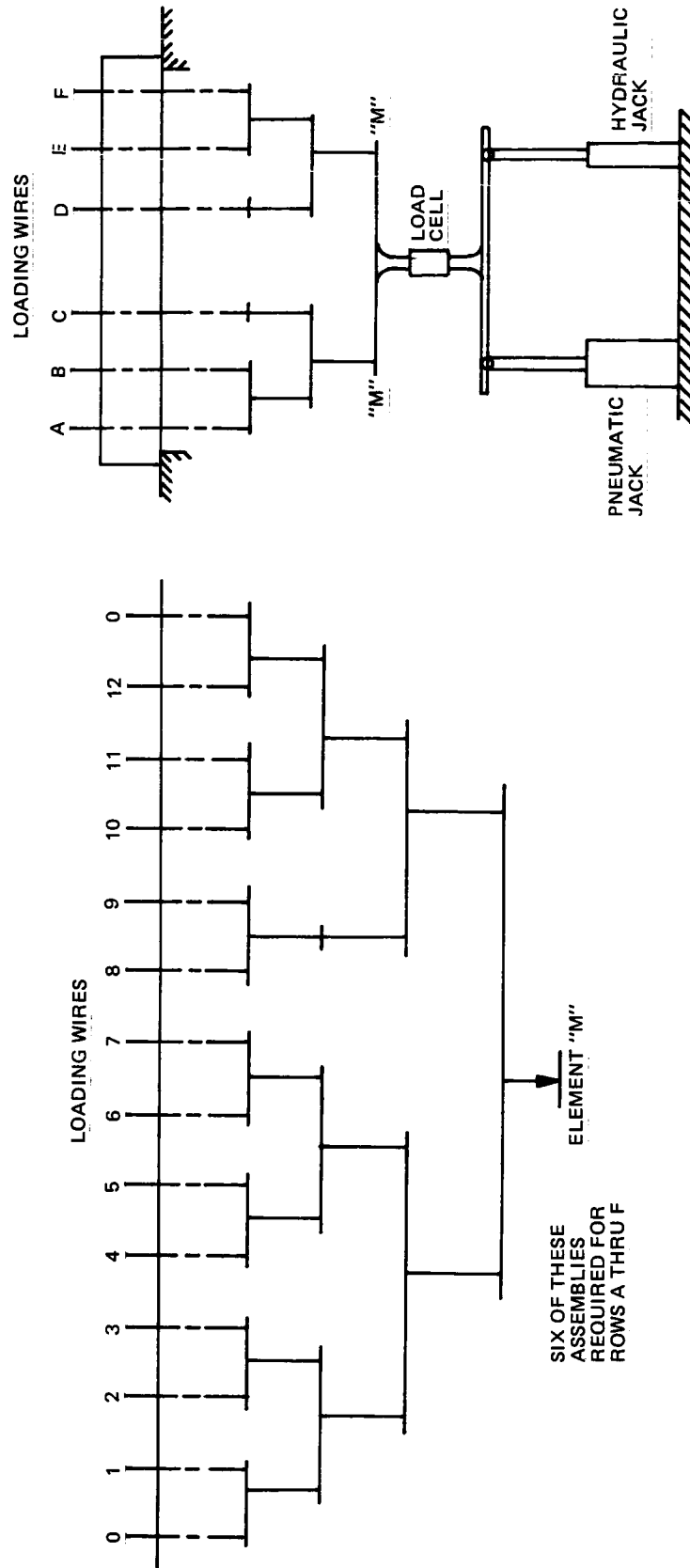


Fig. 4-3 Wiffle-Tree Loading Device

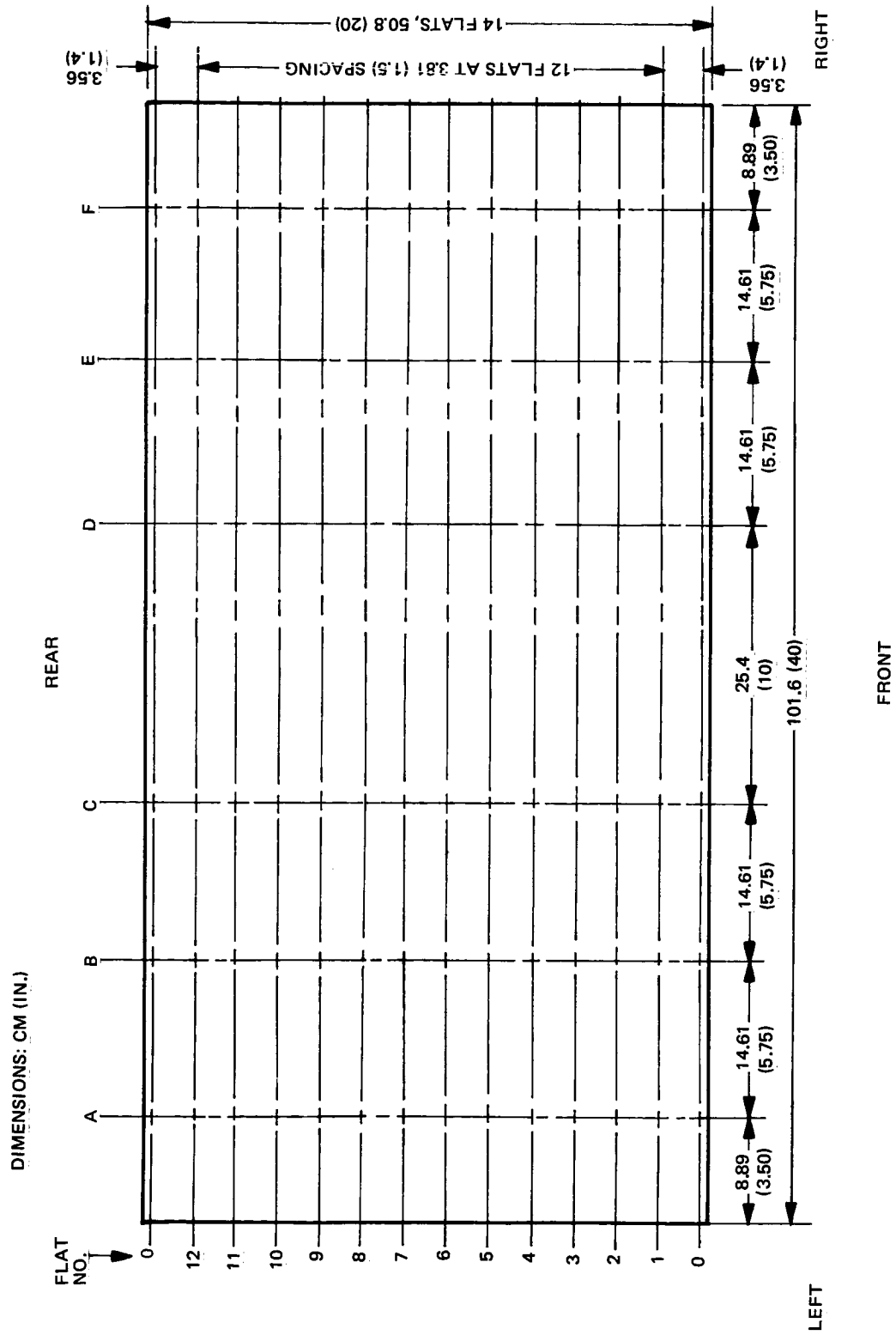


Fig. 4-4 Loading-Wire-Number Locations

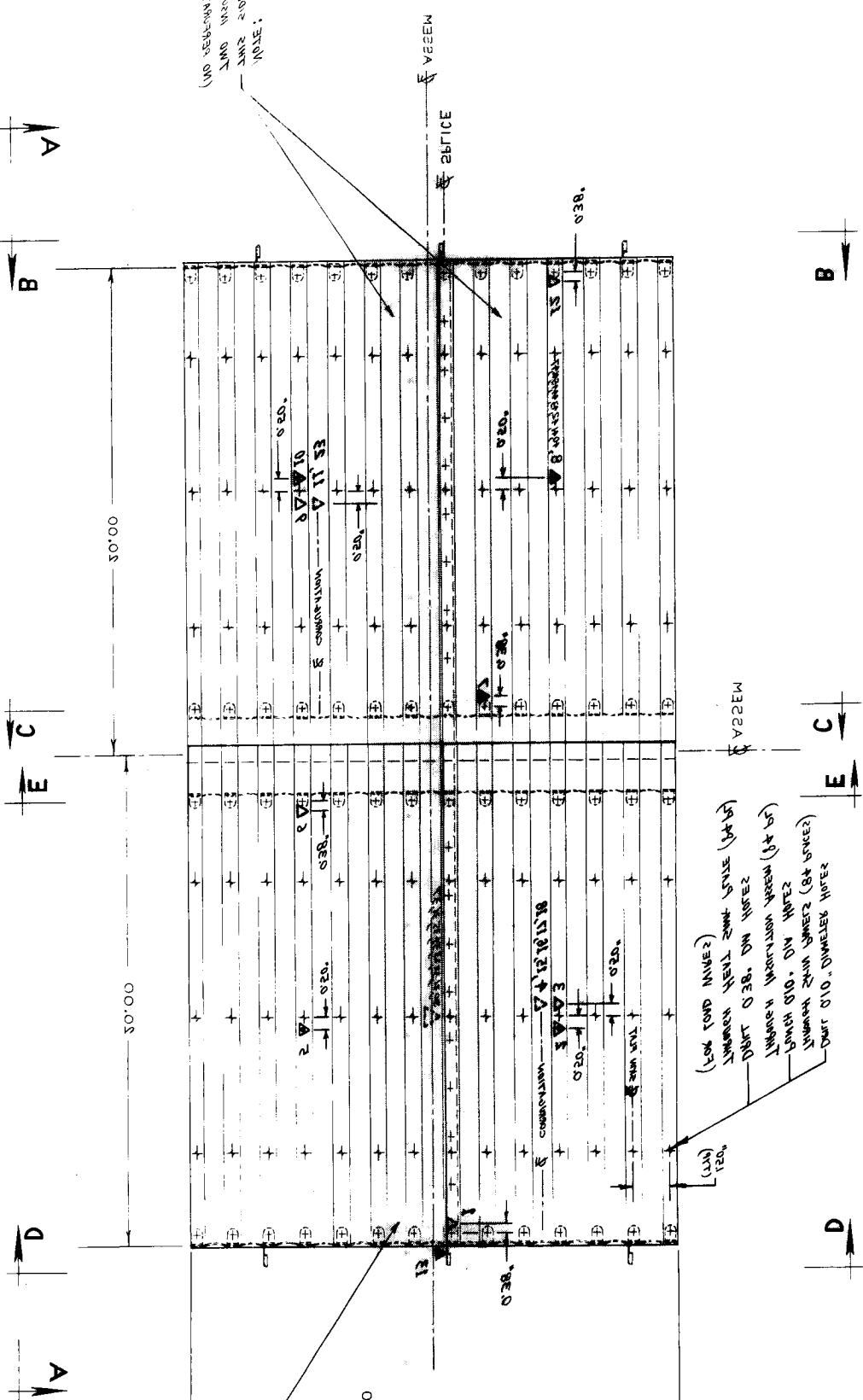
3-3  
TDCS

MEM D-D

NOTE:  
THIS SIDE CONTAINS  
ONE NEGATIVE PAGE  
(WITH HOLEZ FOR FOOD MATEZ)

(FOR TOWN NINE)  
 TOWN OF NINE TOWN NINE (94 15)  
 -DONT 038. ON NINE  
 TOWN OF NINE TOWN NINE (94 15)  
 -DONT 038. ON NINE  
 TOWN OF NINE TOWN NINE (94 15)  
 -DONT 038. ON NINE  
 TOWN OF NINE TOWN NINE (94 15)  
 -DONT 038. ON NINE

DT-DNIC-PT 2PT JMAN9 TEST YJBM32A (WVIV MAJ9) (PLAN VEV)



NOTATION		NOTATION	
1	2	3	4
5	6	7	8
9	10	11	12
13	14	15	16
17	18	19	20
21	22	23	24
25	26	27	28
29	30	31	32
33	34	35	36
37	38	39	40
41	42	43	44
45	46	47	48
49	50	51	52
53	54	55	56
57	58	59	60
61	62	63	64
65	66	67	68
69	70	71	72
73	74	75	76
77	78	79	80
81	82	83	84
85	86	87	88
89	90	91	92
93	94	95	96
97	98	99	100

DATE	NO.	DESCRIPTION	UNIT
1	2	3	4
5	6	7	8
9	10	11	12
13	14	15	16
17	18	19	20
21	22	23	24
25	26	27	28
29	30	31	32
33	34	35	36
37	38	39	40
41	42	43	44
45	46	47	48
49	50	51	52
53	54	55	56
57	58	59	60
61	62	63	64
65	66	67	68
69	70	71	72
73	74	75	76
77	78	79	80
81	82	83	84
85	86	87	88
89	90	91	92
93	94	95	96
97	98	99	100

▲ — BEFORE SURVEY  
 ▼ — SURFACE CONTROL TC  
 ▲ — SURFACE TC

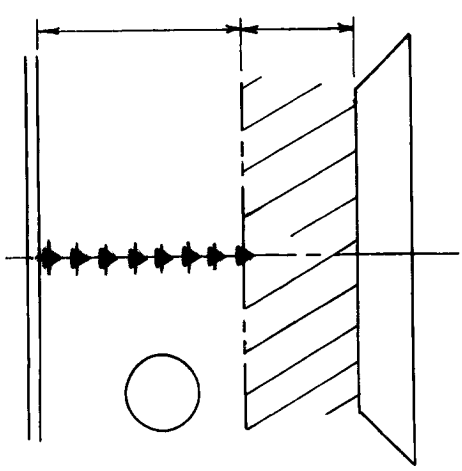
THEMOCOUNTS :

LOAD WIRE: + — — — — — b

NOTATION

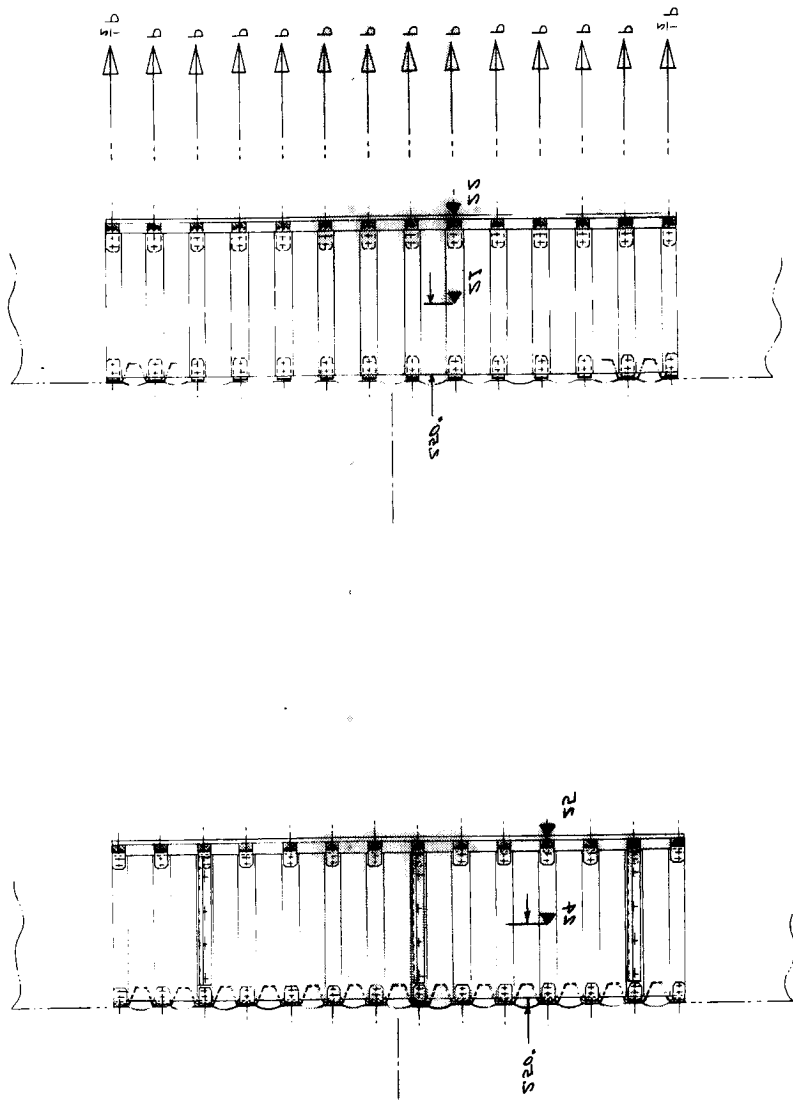
(1) ...  
 (2) ...  
 (3) ...  
 (4) ...  
 (5) ...  
 (6) ...  
 (7) ...  
 (8) ...  
 (9) ...  
 (10) ...  
 (11) ...  
 (12) ...  
 (13) ...  
 (14) ...  
 (15) ...  
 (16) ...  
 (17) ...  
 (18) ...  
 (19) ...  
 (20) ...  
 (21) ...  
 (22) ...  
 (23) ...  
 (24) ...  
 (25) ...  
 (26) ...  
 (27) ...  
 (28) ...  
 (29) ...  
 (30) ...  
 (31) ...  
 (32) ...  
 (33) ...  
 (34) ...  
 (35) ...  
 (36) ...  
 (37) ...  
 (38) ...  
 (39) ...  
 (40) ...  
 (41) ...  
 (42) ...  
 (43) ...  
 (44) ...  
 (45) ...  
 (46) ...  
 (47) ...  
 (48) ...  
 (49) ...  
 (50) ...  
 (51) ...  
 (52) ...  
 (53) ...  
 (54) ...  
 (55) ...  
 (56) ...  
 (57) ...  
 (58) ...  
 (59) ...  
 (60) ...  
 (61) ...  
 (62) ...  
 (63) ...  
 (64) ...  
 (65) ...  
 (66) ...  
 (67) ...  
 (68) ...  
 (69) ...  
 (70) ...  
 (71) ...  
 (72) ...  
 (73) ...  
 (74) ...  
 (75) ...  
 (76) ...  
 (77) ...  
 (78) ...  
 (79) ...  
 (80) ...  
 (81) ...  
 (82) ...  
 (83) ...  
 (84) ...  
 (85) ...  
 (86) ...  
 (87) ...  
 (88) ...  
 (89) ...  
 (90) ...  
 (91) ...  
 (92) ...  
 (93) ...  
 (94) ...  
 (95) ...  
 (96) ...  
 (97) ...  
 (98) ...  
 (99) ...  
 (100) ...

NOTE



VIEW B-B

SECTION C-C



DATE	NO.	DESCRIPTION	UNIT
1	2	3	4
5	6	7	8
9	10	11	12
13	14	15	16
17	18	19	20
21	22	23	24
25	26	27	28
29	30	31	32
33	34	35	36
37	38	39	40
41	42	43	44
45	46	47	48
49	50	51	52
53	54	55	56
57	58	59	60
61	62	63	64
65	66	67	68
69	70	71	72
73	74	75	76
77	78	79	80
81	82	83	84
85	86	87	88
89	90	91	92
93	94	95	96
97	98	99	100

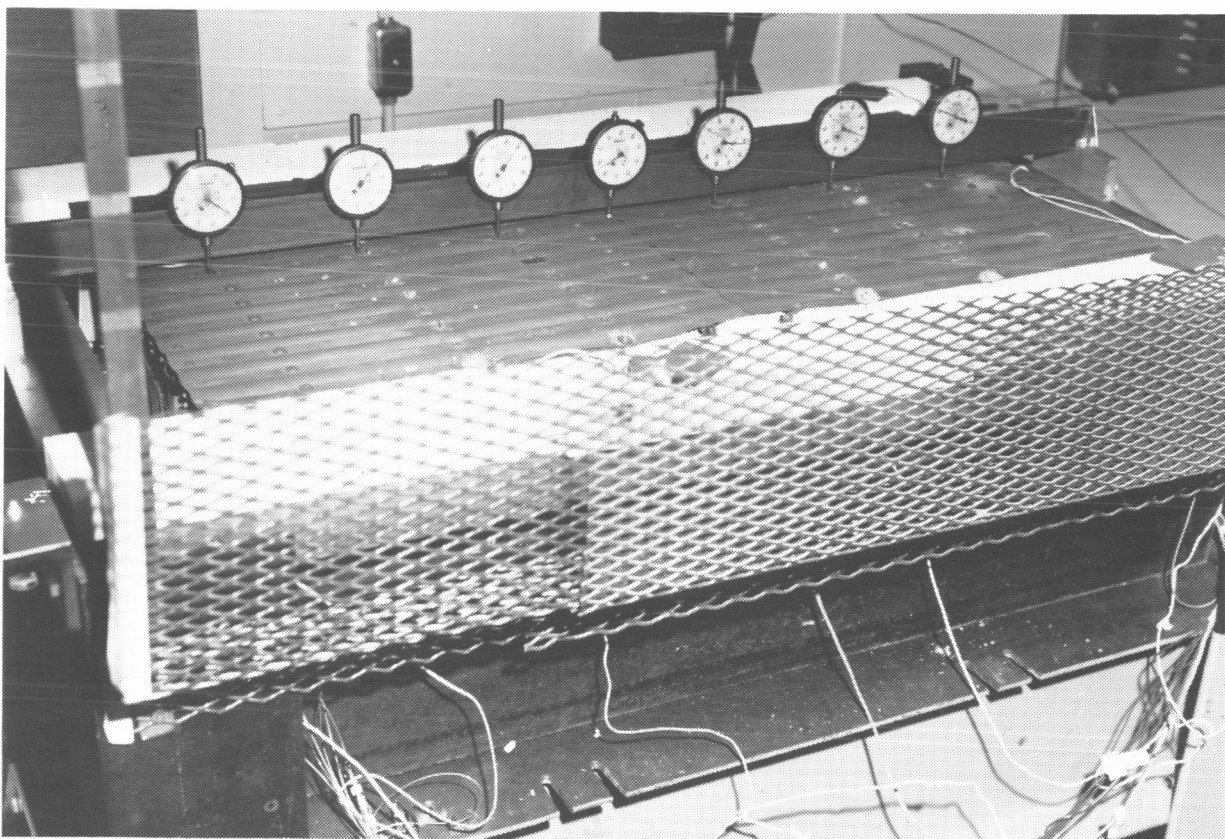


Fig. 4-6 Measuring Bridge

## Section 5

### RESULTS & DISCUSSION

#### 5.1 INITIAL THERMAL CYCLES

The first 10 cycles, which consisted of reentry heating conditions only, were intended to verify the thermal performance of the insulation blanket, to verify the uniformity of the panel surface temperatures, and, in general, to check the heating array and its controller. The heating array performed very well, producing a nearly uniform  $1200^{\circ}\text{C}$  ( $2200^{\circ}\text{F}$ ) over the panel frontface. On a typical temperature cycle, the temperature over six surface thermocouples varied by less than  $60^{\circ}\text{C}$  ( $110^{\circ}\text{F}$ ), from  $1220$ – $1160^{\circ}\text{C}$  ( $2230$ – $2120^{\circ}\text{F}$ ). The peak surface temperatures during cycle No. 2 are shown in Fig. 5-1 at their respective surface locations.

Transient temperature response is shown in Fig. 5-2 for cycle No. 2. Here, the surface temperature is very close to the required value up until about 2200 seconds into the reentry cycle. From this point on, the surface temperature remains higher than the required input due to the presence of the heating array preventing the surface from radiating heat away rapidly enough. Hence, the heating and cooling rates in this apparatus were adequate for the most significant parts of the simulated reentry cycles.

The insulation did not exhibit appreciable degradation during the first 10 cycles, as demonstrated by comparing the backface temperature response of cycles 2 and 10. These are very similar, as can be seen in Fig. 5-3, where plots are presented of the temperature response of the two extremities of the Protecalor and the aluminum backface. The Protecalor maximum temperature did not exceed  $715^{\circ}\text{C}$  ( $1320^{\circ}\text{F}$ ), and the aluminum heat sink never exceeded  $90^{\circ}\text{C}$  ( $200^{\circ}\text{F}$ ).

During an actual reentry mission, some additional benefit is obtained from starting the reentry in a vacuum and flying through an ambient pressure trajectory where the pressure is mostly less than the one atmosphere present during the test. At reduced pressures, the insulation thermal conductivity is reduced, effecting a

reduction in insulation thickness. Considering these points, reduction in the Dynaflex thickness appears to be in order, and perhaps some reduction in the Protecalor thickness is possible as well.

Figure 5-4 shows a typical temperature response through the Protecalor insulation, which in this case is cycle 2. Thermocouple No. 30 is located on the bag surface and thermocouples 31-37 are on the seven radiation foils.

Temperatures on the flexing support rib are shown in Fig. 5-5 and are taken from cycle No. 2. They are typical of all support rib results. Note that the peak temperature for TC 19 is 677°C (1250°F), about the same value as the insulation temperature at the identical depth relative to the frontface. The heat leakage through the support ribs was apparently of manageable proportions.

## 5.2 THERMAL-STRUCTURAL CYCLES

Following cycle No. 10, the whiffle-tree loading apparatus was installed so that static pressure loading could be applied to the test article. From this point on, the cycles consisted of cold static pressure load followed by combined reentry temperature and pressure loads. For the first combined-environment test, cycle No. 11, only 80% of the peak static load was applied. Subsequently, 100% load was applied on each cycle.

### 5.2.1 Panel Thermal Response

Insertion of the loading wires from the frontface structure through the insulation blanket raises the insulation's effective thermal conductivity, and should increase the temperature response of the insulative system. By comparing the temperatures of cycles 2 and 12, as shown in Fig. 5-6, it can be seen that the loading wires raise the backface temperatures by about 8°C (15°F), a small amount not significantly affecting panel behavior. Continuing the testing through additional cycling did not further degrade the insulation, as can be seen by examining Fig. 5-7. Here, internal insulation blanket temperature responses for cycles 17 and 77 are compared and found to be nearly identical. These temperature response curves are typical for all cycles; therefore, the data for all the other cycles will not be given here. Again, it is

pointed out that the Protecalor did not reach its allowable peak temperature of 900°C (1650°F), and that further insulation weight reduction is possible.

During the first 14 thermal cycles, numerous failures of the frontface thermocouples occurred. These failures were due to excessive oxidation of the unjacketed thermocouple leads. Because replacing or repairing these instruments was very time-consuming, it was decided to introduce "floating" thermocouples to the frontface. These floating thermocouples consisted of jacketed thermocouples embedded in a flat piece of ceramic material called CPI. The ceramic pieces were rectangular, approximately 3.8 by 3.8 by 0.3 cm (1-1/2 by 1-1/2 by 1/8 in.), and were merely laid on the top surface of the panel. Five of these were placed on the surface at the approximate locations of thermocouples 2, 5, 7, 8, and 9. To determine their suitability, their temperature outputs on test run No. 15 were compared with the two remaining original, Dassault-installed thermocouples, No. 9 and 10, as plotted in Fig. 5-8. Here, it is observed that at the higher temperatures there is good agreement, but for some reason, below 930°C (1700°F), the two original TCs did not give any output. Because the temperature response was adequate and the higher temperatures agreed, it was decided to continue with the floating thermocouples for the remainder of the test program.

#### 5.2.2 Flatness Measurements

Following temperature cycle No. 10, the whiffle-tree loading device was installed and a load-deflection survey of the panel was made. This survey was performed by placing the measuring bridge used for the flatness surveys on flat No. 7, and incrementing the static load by 45 kg (100 lb). After a peak load of 440 kg (967 lb) was obtained, the panel was unloaded and another zero measurement taken. (See Table A-1 in the Appendix.)

Figure 5-9 presents mid-span deflection versus load along flat No. 7. Prior to any loading, the initial zero-load-point deflection measurement was zero for both left and right spans. After loading, the left-span deflection data indicated that some settlement had occurred; i.e., the extrapolated data gave a zero-load displacement of 0.038 cm (0.015 in.). A subsequent left-span zero-load deflection measurement

of 0.04 cm (0.016 in.) verified this settlement. It is necessary to subtract this initial settlement (the 0.038-cm (0.015-in.) value was used) from the left span of each subsequent flatness survey.

A comparison of the data with a theoretical deflection curve is also shown in Fig. 5-9. Note that the theoretical line has a smaller slope than the data line. The theoretical curve assumes that the span is a simply supported beam with no rotational end restraints. This is not exactly true, as the support ribs do provide some rotational end restraint.

Flatness surveys were made at various intervals to measure the permanent set caused by plasticity effects - primarily, high-temperature creep. Flatness survey data for the mid-span points along flats No. 4 and 9 are plotted in Fig. 5-10 as functions of the number of test cycles. Here, the initial support settlement is subtracted from the left span. However, the left span has a greater permanent deflection than the right. This is probably due to the fact that the temperatures over the left span were slightly higher than those on the right, and caused more creep to occur in the beads and corrugations. It is observed that there is measureable permanent deflection after the first 10 cycles, in spite of there having been no pressure load applied. This is probably due to the effect of residual stresses built into the panel during manufacture and assembly combined with the thermal stresses produced by the applied heat load.

There is another significant increase in permanent deflection of the left span and a rearrangement of permanent deflection in the right span between cycles 10 and 19. This is apparently due to residual stress acted upon by the applied mechanical load introduced in cycle 11, as well as the thermally induced loads. The residual stress distributions are altered by the application of the simulated pressure load. From cycles 19 to 100, the increase in permanent deflection is more orderly and is indicative of the behavior which results from cyclic creep. This phenomenon was observed during cyclic testing of Haynes-25 panels by Grumman and is reported in Ref 7 and 11. Note that the magnitude of these permanent deflections is relatively small in all cases.

Figure 5-11 shows the permanent deflection plotted in the spanwise direction for flat No. 4, a typical flat. Here, again, the difference in deformation between the left and right spans is illustrated. This type of behavior was also observed during cyclic testing of Haynes-25 panels and was reported in Ref 7 and 11.

A combination of 100-cycle permanent set plus deflection produced by a limit cold static load of  $144 \text{ N/m}^2$  (3 psi) is shown in Fig. 5-12. It can be seen that the maximum allowable deflection, 1.27 cm (0.5 in.), provides ample margin for this parameter. This is the maximum deflection obtained at any time during a 100-mission life under limit load. It appears that this panel configuration and material were successful in preventing excessive cyclic creep at temperatures up to  $1200^\circ\text{C}$  ( $2200^\circ\text{F}$ ).

### 5.2.3 Additional Test Results

A log of all the test cycles is presented in Table 5-1, where dates and comments on loads and anomalies occurring during the testing are included. There were a number of loading-wire failures that were reported. These consisted of the wire breaking in the vicinity of the washer connecting it to the hot TPS panel frontface. It is probable that these failures were due to creep rupture and excessive oxidation of the wires occurring in the  $1200^\circ\text{C}$  ( $2200^\circ\text{F}$ ) environment. The loading wires were made of Haynes-25 and Haynes-188, alloys not suitable for this temperature. TD Ni-20Cr wire, if available, would be a better material.

There were numerous runs where a few loading wires failed. When this happened, the loads from the failure load point were added to the adjacent load point in the same lettered row, and the panel still carried the same total load. However, concentrated stresses around the overloaded hole were now twice as large. In seven cases, an entire lettered row failed and the load was terminated before peak hot-pressure load was attained.

At the conclusion of the 88th cycle, a 3.8-cm (1-1/2-in.) crack was observed along flat No. 7, in the vicinity of load link C-7. The crack was along the intersection of the flat and the bead and right around a loading point. A picture of the crack is shown in Fig. 5-13. There are a number of stress concentrations interacting at this location: there is a large thermal stress due to the flexing of the bead, there is a stress concentration from load point C-7, and there is a stress concentration from

the fasteners making the lateral joint running along flat No. 7. Probably, this crack was present for a number of cycles before it was discovered. It was decided to replace the 1.27-cm (0.5-in.) diameter washer at the load point with a larger, rectangular one, and continue the test. This washer was 1.3 by 2.5 cm (0.5 by 1.0 in.).

After cycle No. 93, additional cracks appeared in the vicinity of loading points B-7 and C-5. These cracks were also parallel to the beads and near the intersection of the bead and flat. The testing was continued to 100 cycles, again because the load-carrying capability of the panel remained intact.

### 5.3 POST-TEST INSPECTION

The panel was photographed (Fig. 5-14) on the test rig after 100 cycles had been completed. The metallic frontface had a thin layer of greenish-black powder over the entire surface. Upper side surfaces were discolored and had a greenish hue.

After removal from the test rig, additional photographs (Fig. 5-15 and 5-16) were taken of the front and back surfaces, respectively. There were no analyses or high-resolution photos made, nor x-ray diffraction techniques used, to assess the levels of oxidation formed on the surfaces.

It is assumed for this high-temperature static test that:

- Those surfaces exhibiting a greenish hue show the formation of oxidized chromium,  $\text{Cr}_2\text{O}_3$
- The frontface shows  $\text{Cr}_2\text{O}_3$  powder, perhaps becoming dissociated and mixed with  $\text{ThO}_2$  particles (Ref 20)

Five major cracks and a minor crack were observed on the metallic frontface. A map showing the location of these cracks is shown in Fig. 5-17. Note that all the cracks run parallel to the beads and that all the major cracks, those longer than 0.625 cm (1/4 in.), lie at the junction of a flat and a bead in the vicinity of a loading point. There is a stress concentration at these points due to the introduction of the concentrated load from the loading wires. These stresses are added to the stress in the bead, which occurs when the bead flexes to take up the thermal expansion in the lateral direction. It is possible that if the load was a uniform pressure instead of a

pattern of discrete concentrated loads, most of the cracking in the facesheet would not have occurred. Recall that the first large crack was observed after the 88th cycle. In spite of the cracking, however, catastrophic failure did not occur, and the panel continued to sustain the applied loads and temperature.

A photograph of the 7.6-cm (3.0-in.) crack located at loading point C-7 is presented in Fig. 5-18. This is the largest crack in the panel and was the first one detected (after cycle 88). Also visible is the 3.6-cm (1.4-in.) crack located at loading point C-5.

The supports at the ends of the panel were designed to take out horizontal loads. This is accomplished by inclusion of drag brackets situated along these supports at a 19-cm (7.5-in.) pitch. For this test article, the supports at the left and right ends had three drag brackets each. The drag bracket comes up to about 1.3 cm (1/2 in.) of the top of the support, and provides no stiffening above this point. It was observed that just above two of the drag brackets on the left end support there were kinks in the support indicating a large horizontal force to the left was sustained there.

A photograph of the kink above the center drag bracket is shown in Fig. 5-19. The horizontal force may have been due to failure of the expansion joint in the center of the panel to allow free expansion. During panel heating, the temperature gradient through the corrugation can produce bowing upward of the panels and consequent pressure between the overlapped beaded sheets in the expansion joint. Hence, thermal expansion could produce a horizontal force in the proper direction to create the noted kinks.

An attempt was made to remove the TD Ni-20Cr threaded fasteners holding the frontface structure to the vertical supports. The fasteners proved to be impossible to remove, probably due to diffusion bonding of the fasteners to the 0.025-cm (0.010-in.) sheet material. In fact, a wrench and screwdriver were unable to open the fasteners at all. If it is required that these fasteners be removable during the service life of the TPS, a potting compound about the fastener should be used. Alternatively, preoxidation of fastener and fastened materials might be investigated to prevent this bonding.

The insulation package was removed from the test panel and examined. Photographs were taken and are presented in Fig. 5-20 and 5-21. The Dynaflex showed considerable shrinkage - about 7% - along the top surface where it was operating at 1200° C (2200° F) and considerably less at lower temperatures. For the test article, the shrinkage reduces rapidly as distance from the 1200° C surface increases, and is negligible at the backface of the Dynaflex, which is 4.0 cm (1.57 in.) from the top surface.

Considerable oxidation of the Inconel bagging around the Protecator was visible, extending from the top surface, where the Dynaflex meets the Protecator, to about one-third of the way down the sides. However, no holes in the foil were found. One side of the bagging was removed to examine the Protecator. Both the reflective screens and the Astroquartz appeared to be in excellent condition. No damage was observed on the polyimide-foam backface bagging.

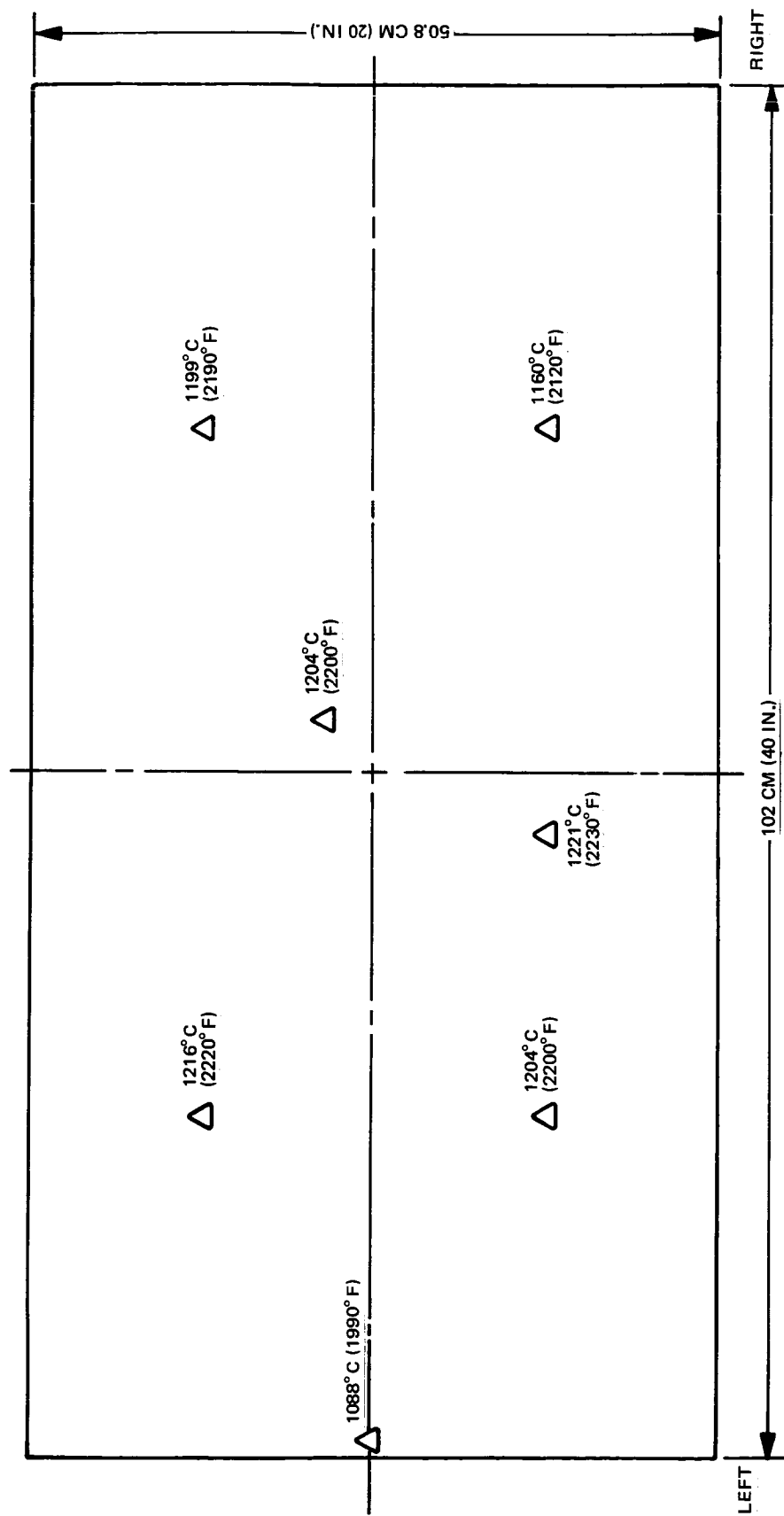


Fig. 5-1 Maximum Surface Temperatures Map

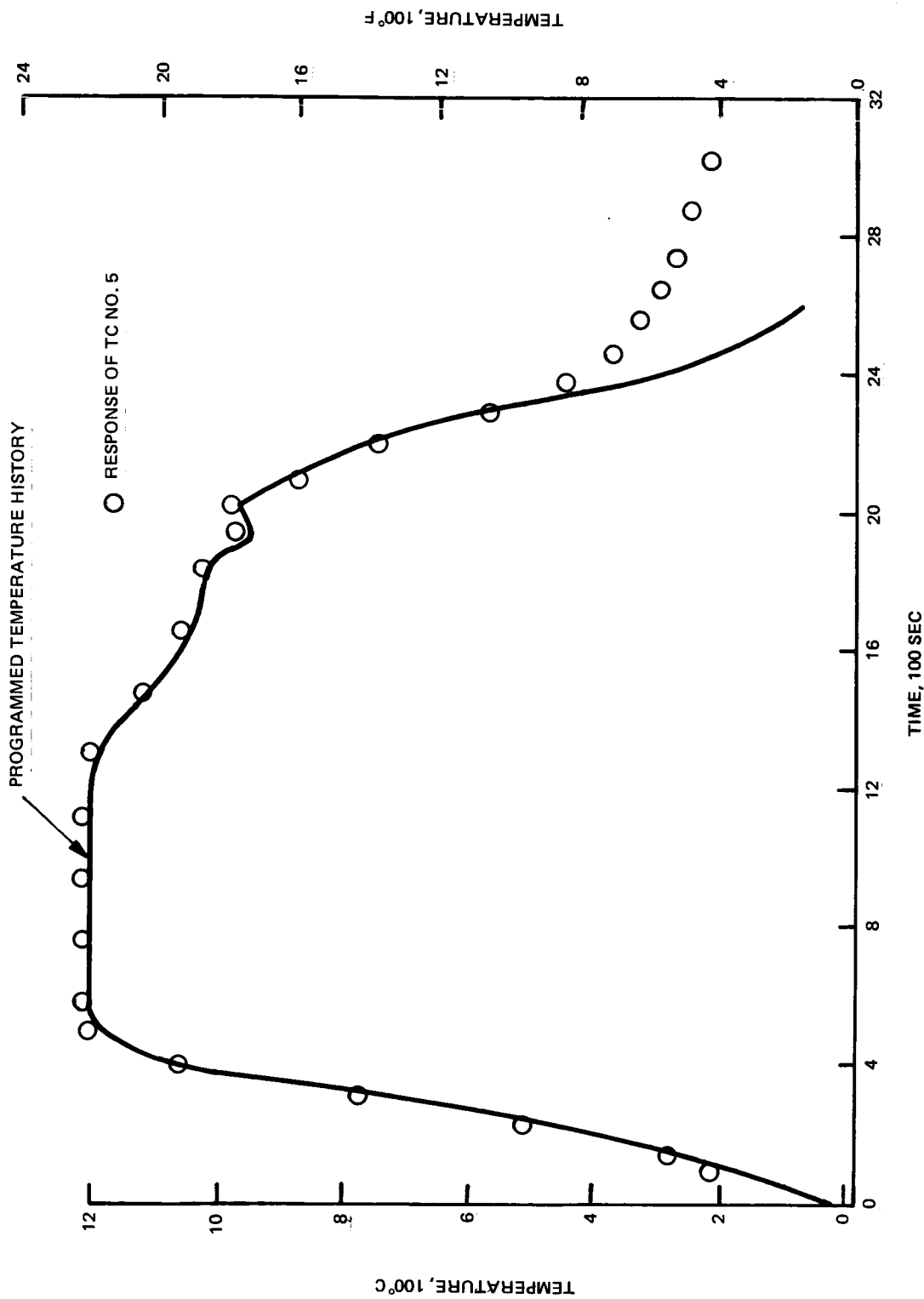


Fig. 5-2 Frontface Temperature Response

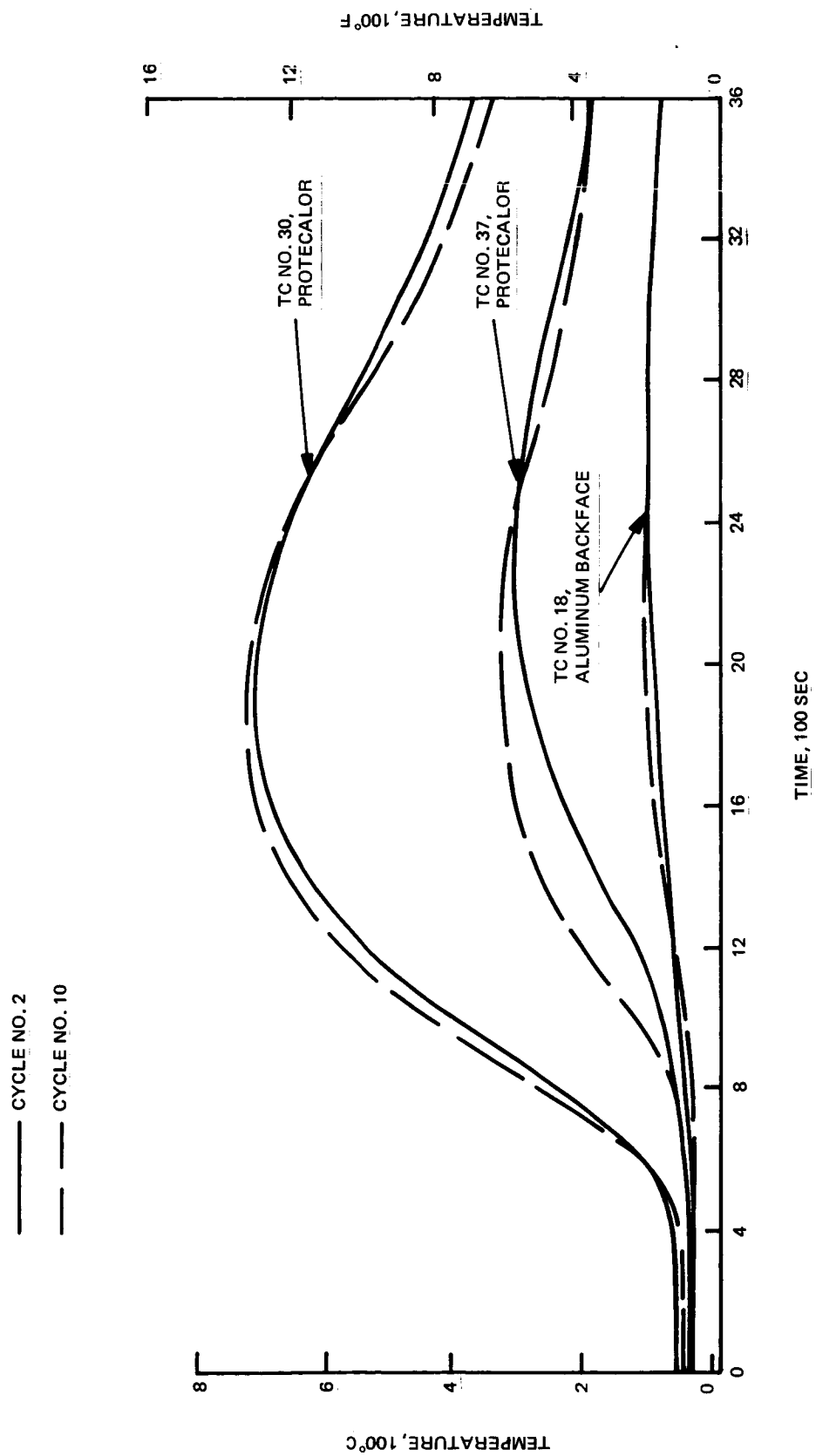


Fig. 5-3 Insulation Temperature Response—Effect of Thermal Cycling

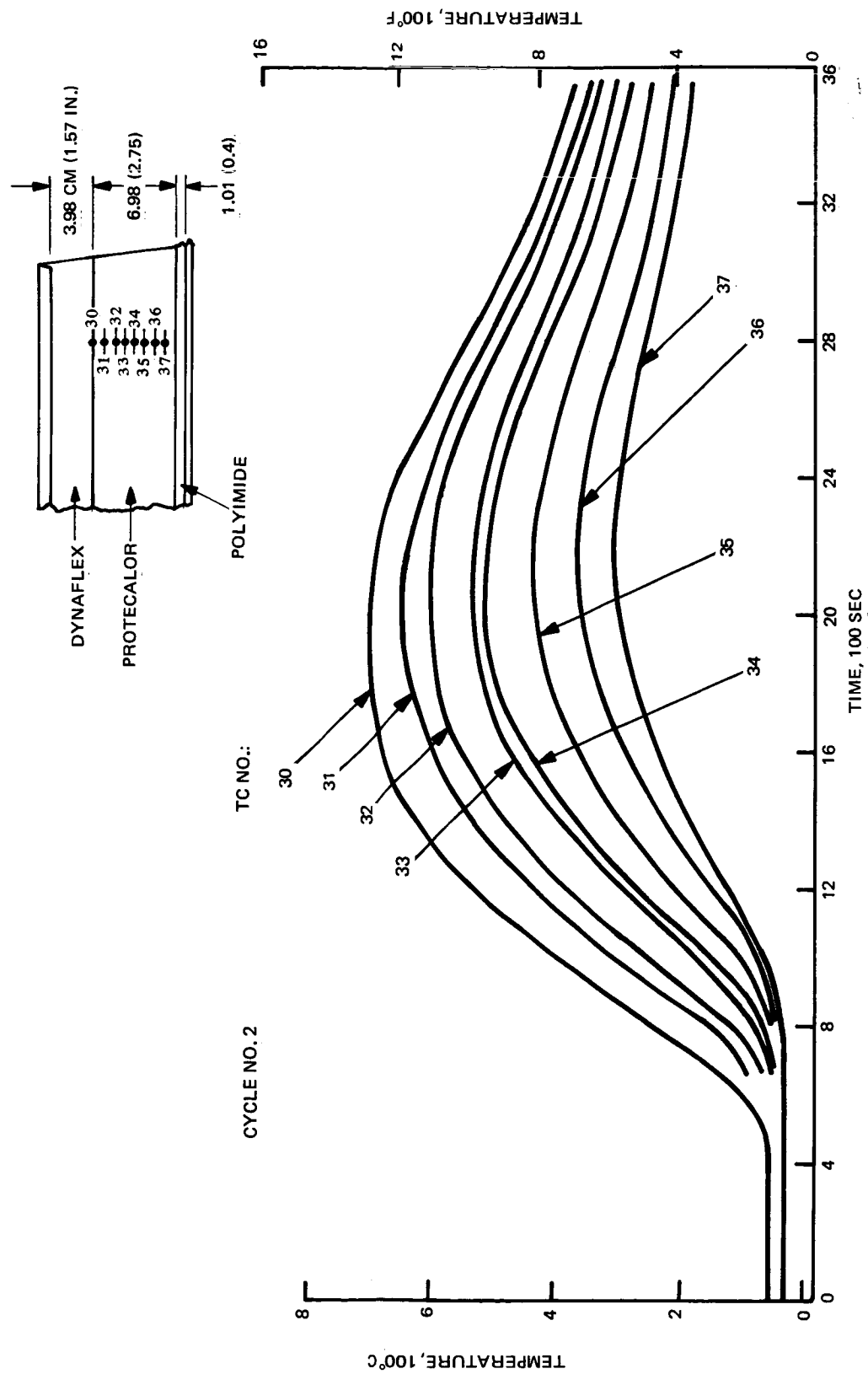


Fig. 5-4 Temperature Response Through Insulation - Cycle No. 2

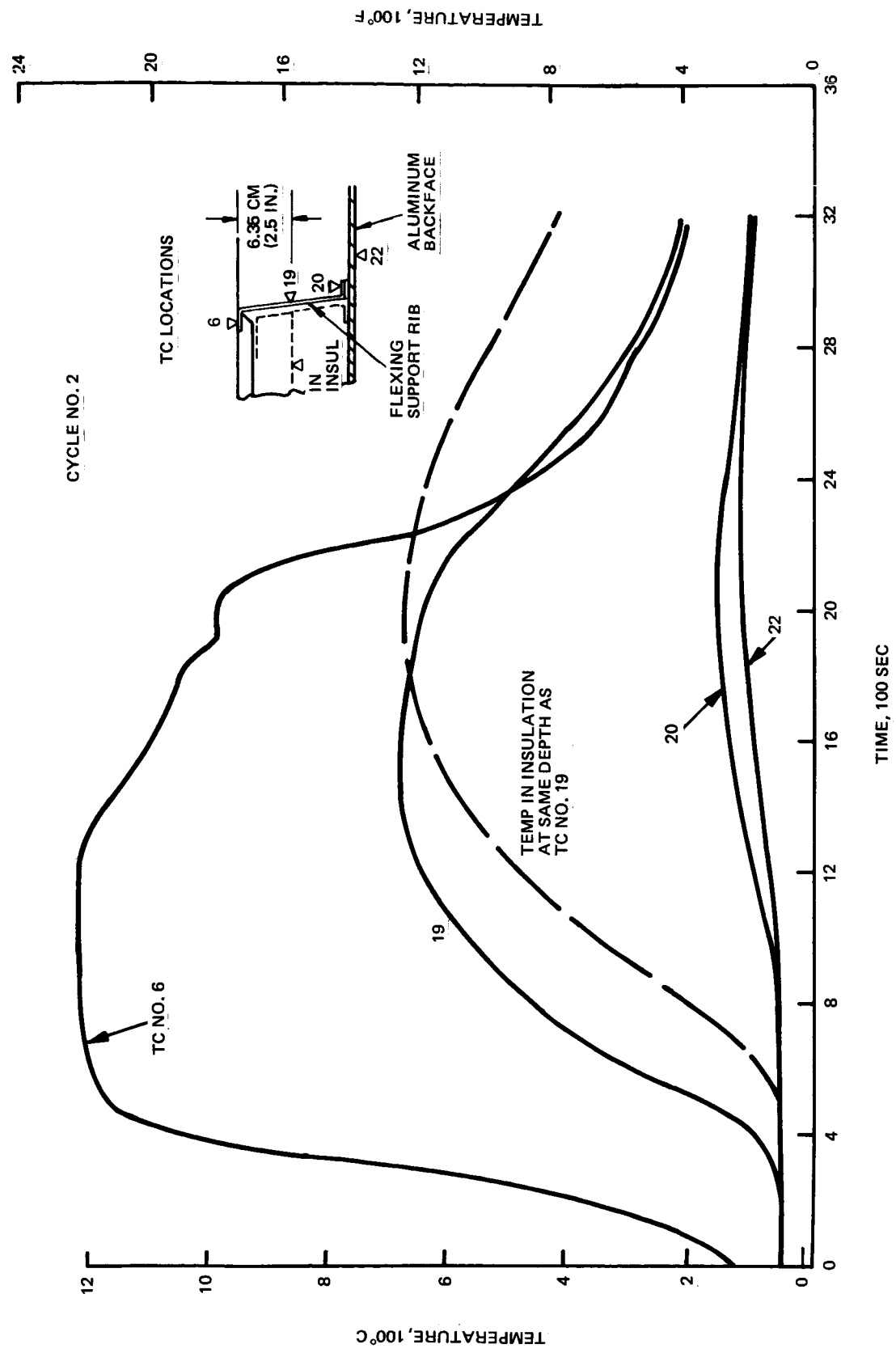


Fig. 5-5 Support Rib Temperature Response

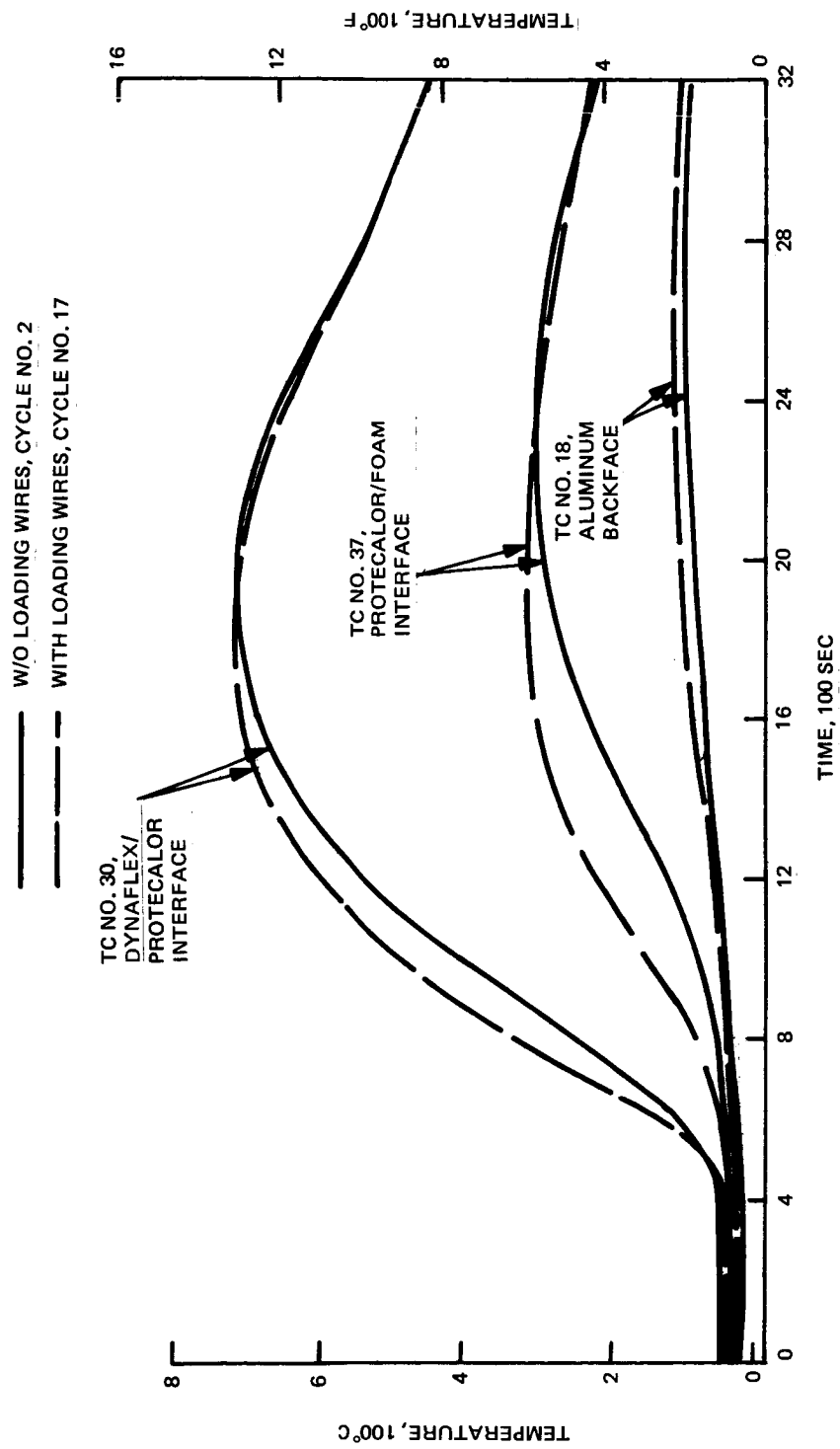


Fig 5-6 Effect of Inserting Loading Wires on Insulation Temperature Response

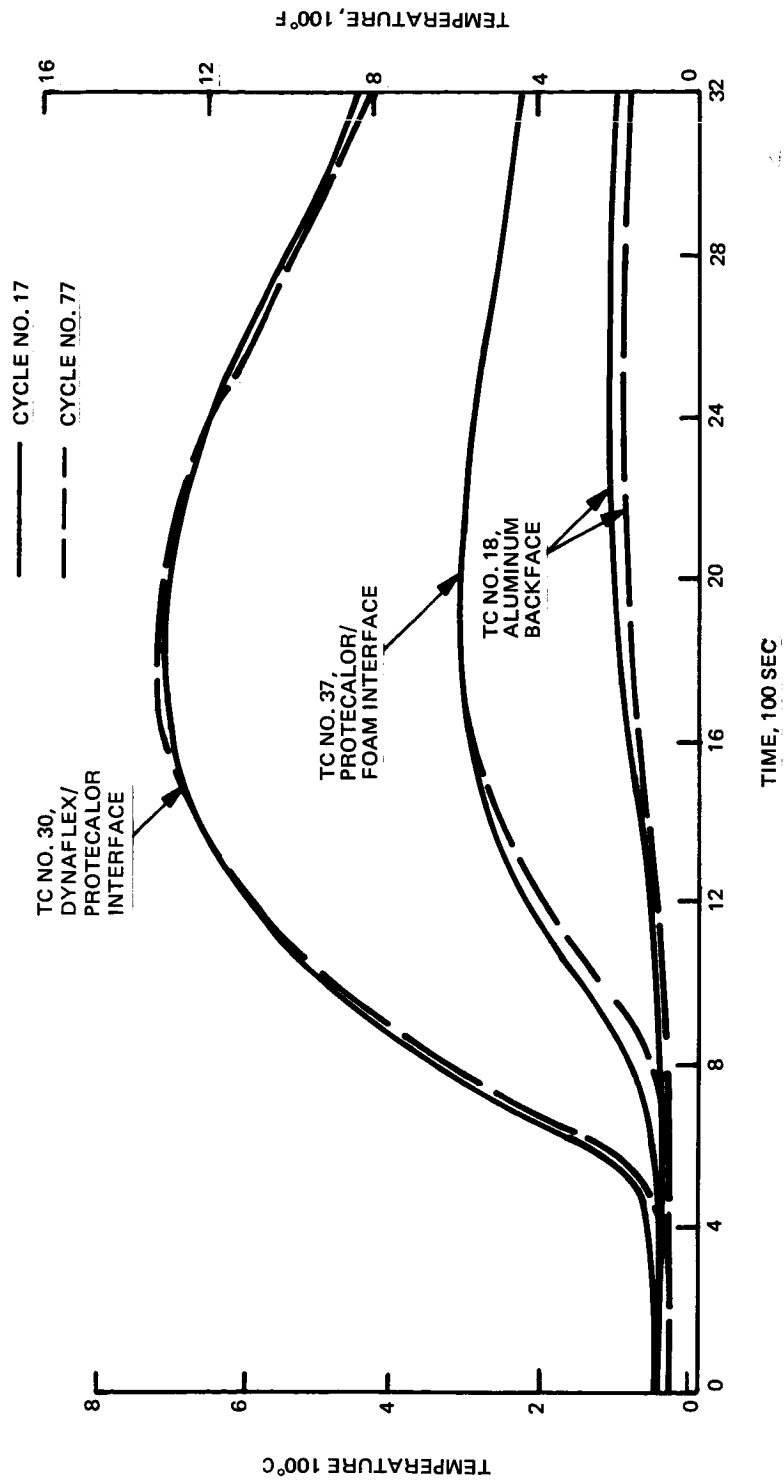


Fig. 5-7 Effect of Repeated Reentry Cycles on Insulation Temperature Response

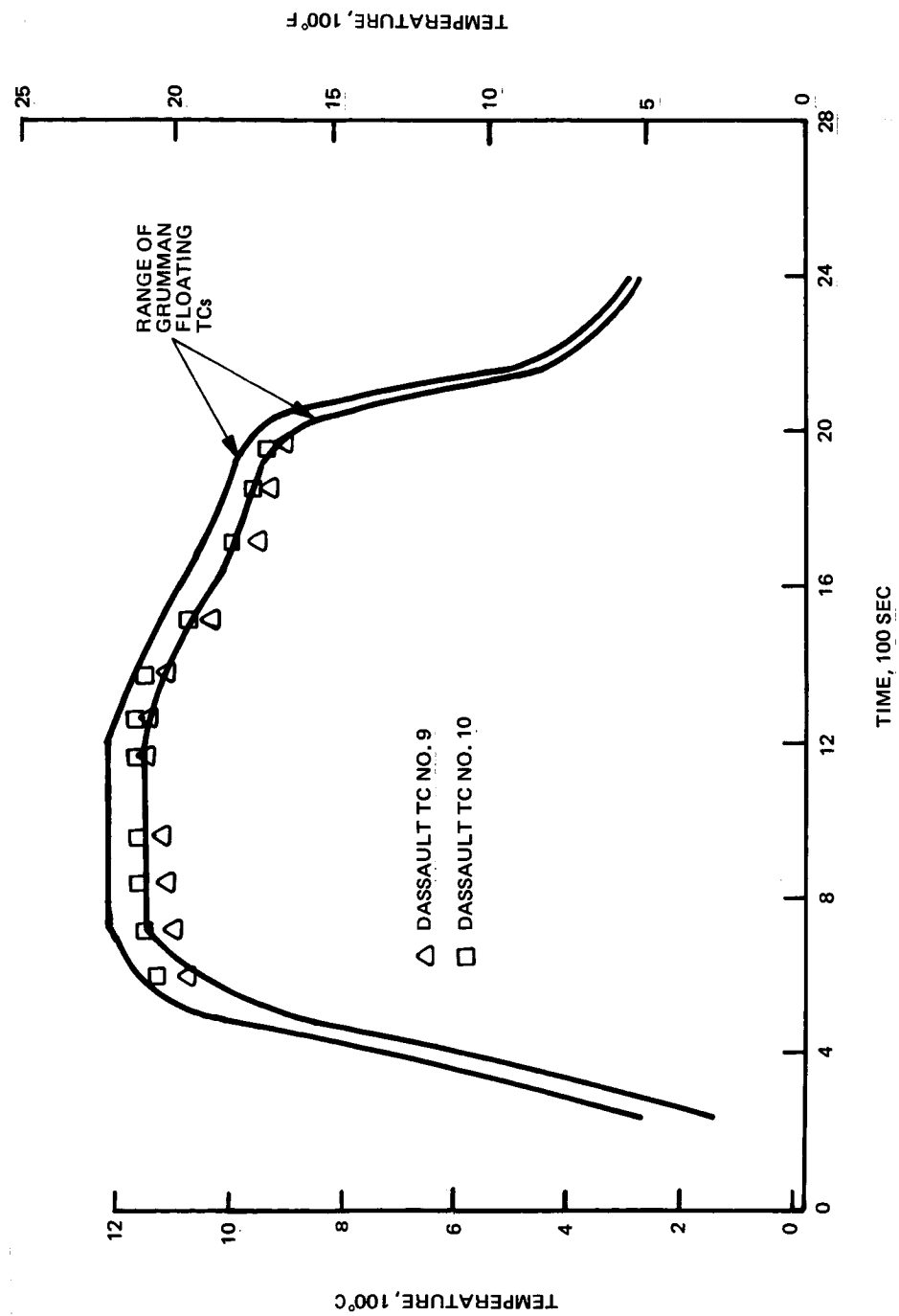


Fig. 5-8 Dassault-Installed & Floating Thermocouple Comparison, Run 15

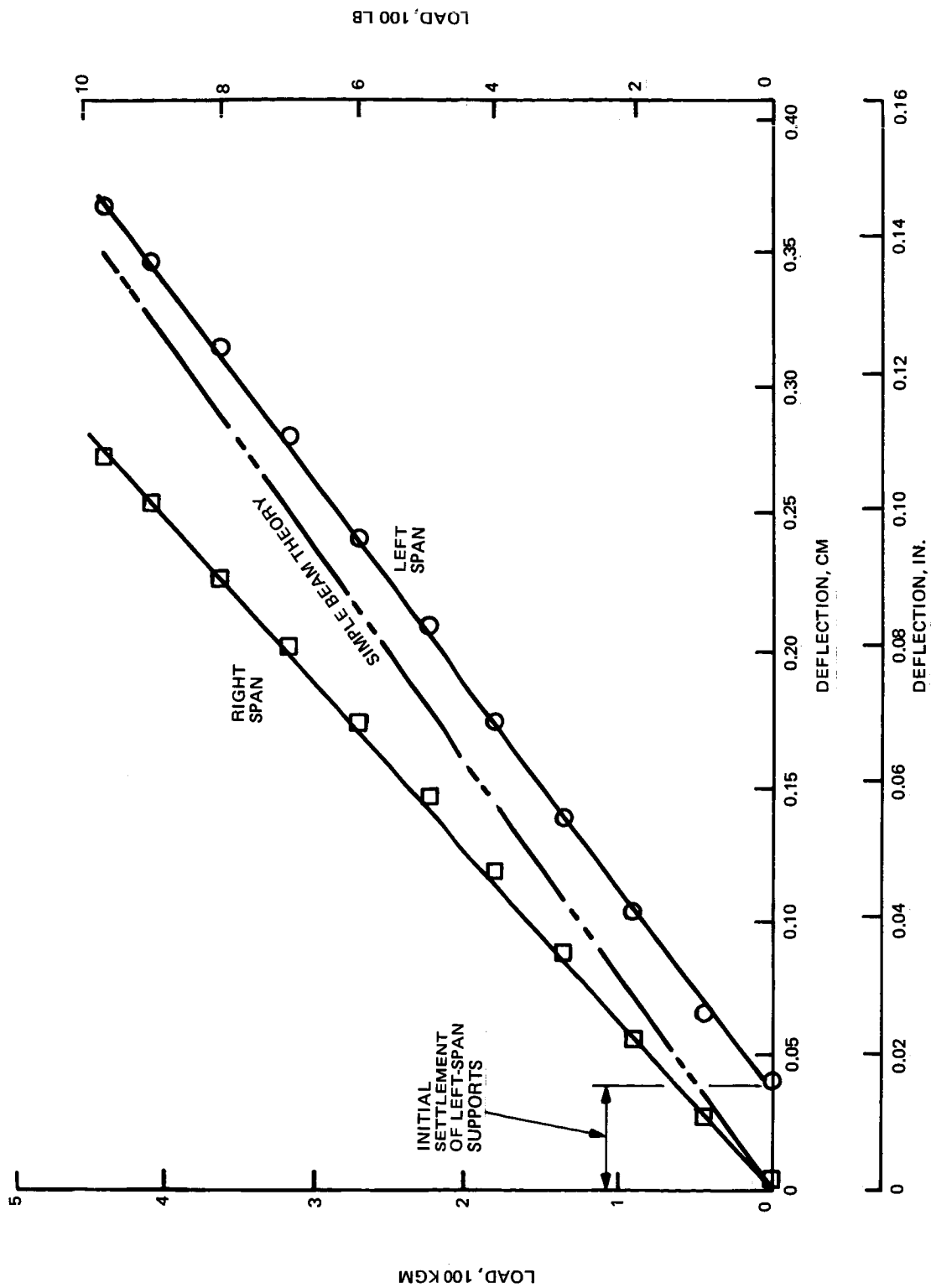


Fig. 5-9 Load-Deflection Survey, Flat No. 7, Midspan

	FLAT NO.	DIAL INDIC NO.	LOCATION
△	4	2	LEFT SPAN
◻	4	6	RIGHT SPAN
○	9	2	LEFT SPAN
◻	9	6	RIGHT SPAN

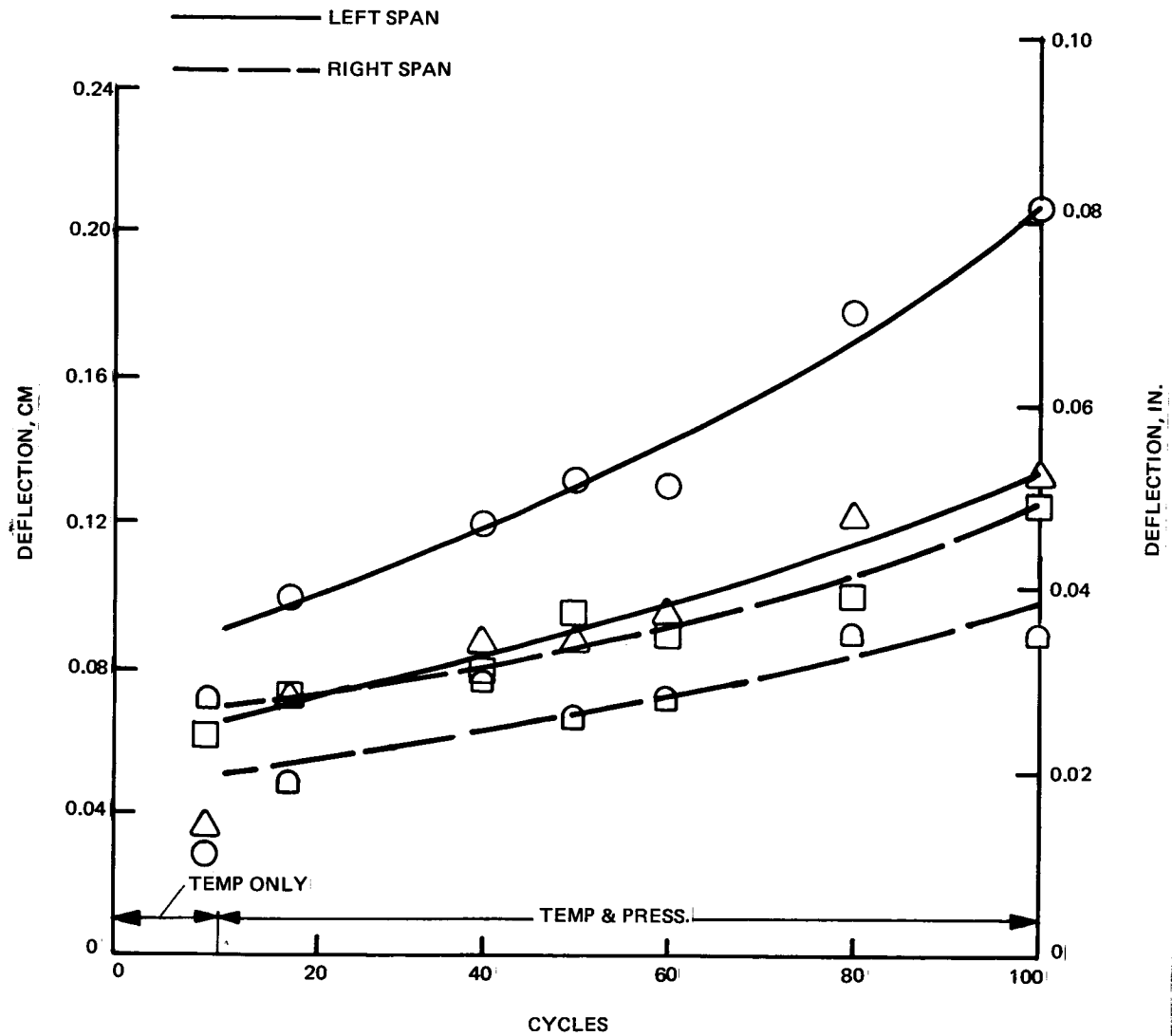


Fig. 5-10 Permanent Deflection, Midspan

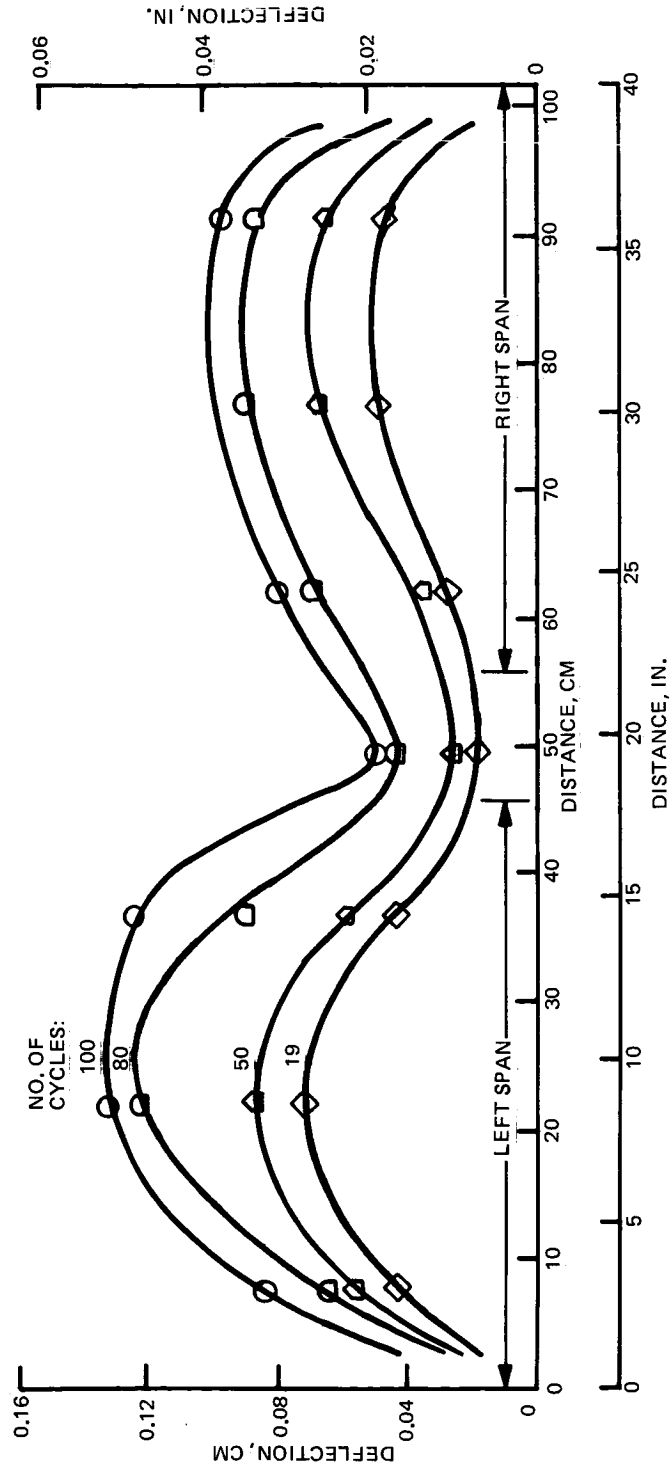


Fig. 5-11 Permanent Deflection, Flat No. 4

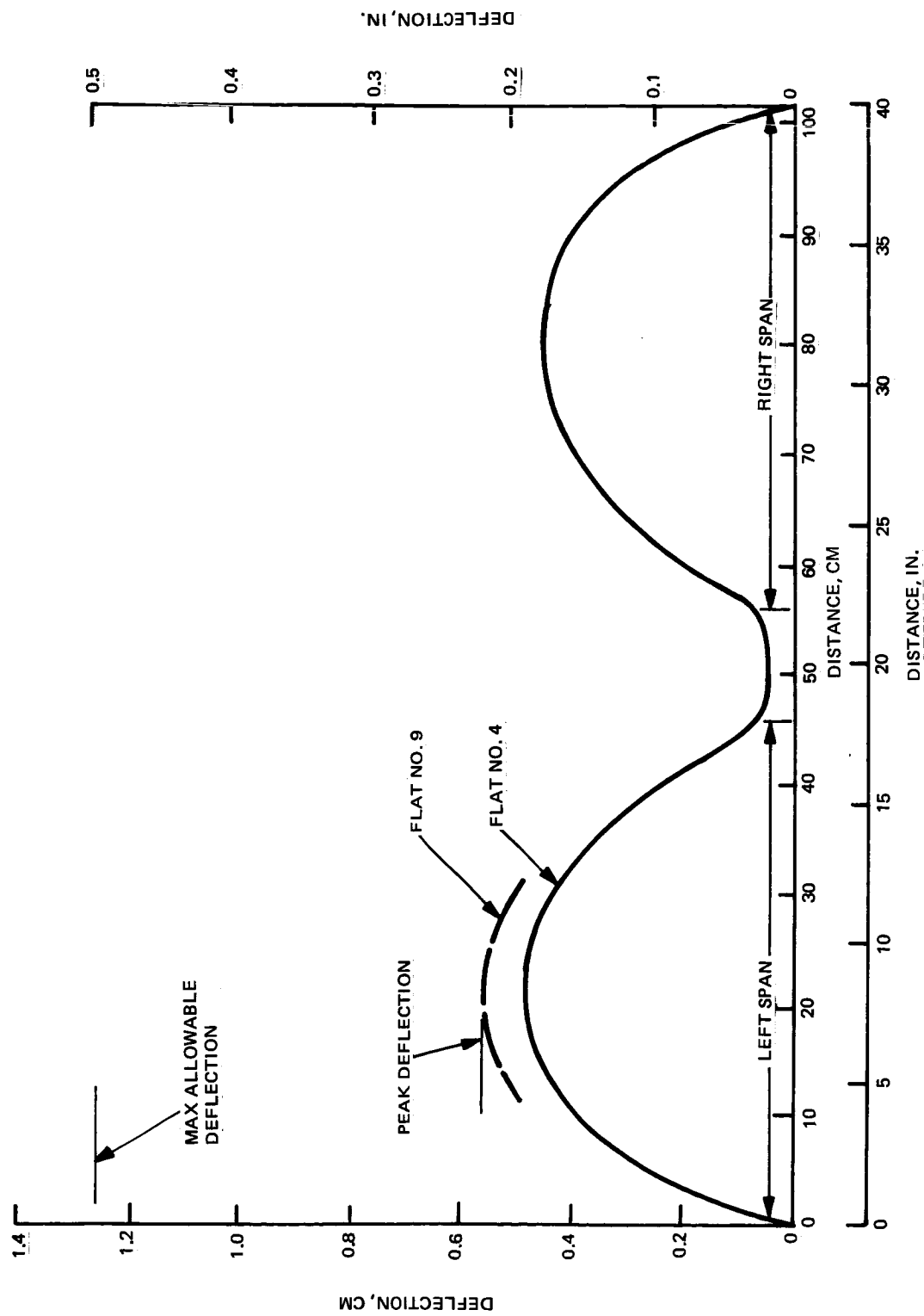


Fig. 5-12 Maximum Deflection, Limit Room Temperature Pressure Plus 100-Cycle Permanent Set

Table 5-1 Test Log (Sheet 1 of 3)

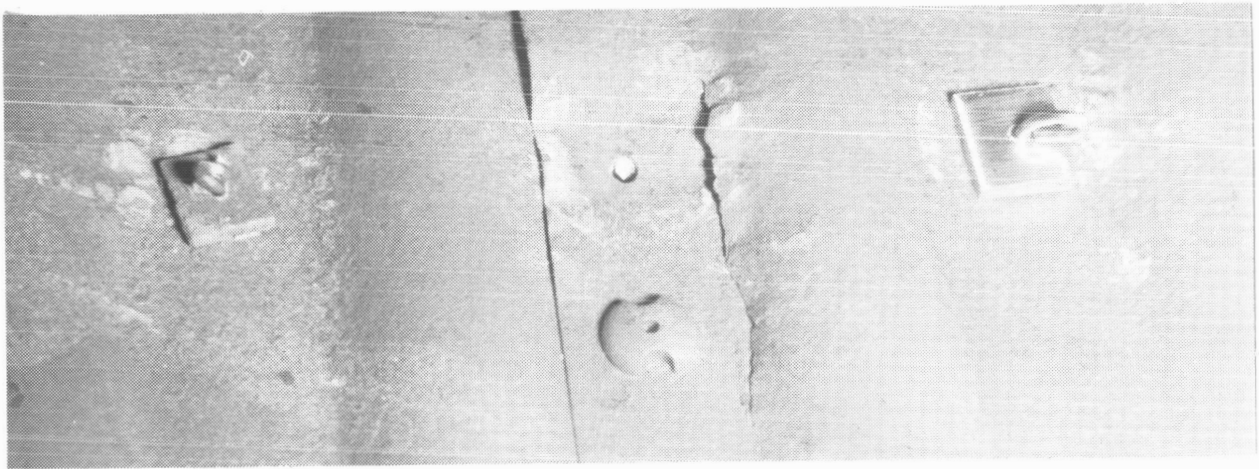
Cycle	Date	% of Peak Hot Load Achieved	Loading Wires Failed	Remarks
1	7-25	0		Peak temp reduced 2 min early
2	7-26	0		
3	7-26	0		
4	7-27	0		TC 6 failed
5	7-27	0		
6	7-27	0		TC 2 failed
7	7-30	0		
8	7-30	0		
9	7-30	0		TC 11 failed
10	7-31	0		8 TCs failed, all on frontface
11	8-21	80		
12	8-22	100		TC 4 failed
13	8-22	100		
14	8-22	100		
15	8-23	100		Introduced "floating" TCs
16	8-23	100		
17	8-23	100		
18	8-24	100	8 in Row B	
19	8-24	100		
20	8-27	104	2 in Row B	
21	8-28	100	1 in Row A	
22	8-28	85		
23	8-29	100		
24	8-29	100		TC 2 & 7 failed
25	8-30	100	1 in Row B	
26	8-30	100		
27	8-31	100		
28	8-31	100		
29	8-31	100	1 in Row B	
30	9-4	100		TC 7 failed, burned hole in skin
31	9-4	100		
32	9-4	100	2 in Row B	
33	9-5	100		
34	9-5	100	2 in Row B	
35	9-5	100	2 in Row B	
36	9-6	100		TC 5 failed
37	9-6	100		
38	9-6	100		
39	9-7	100		

Table 5-1 Test Log (cont) (Sheet 2 of 3)

Cycle	Date	% of Peak Hot Load Achieved	Loading Wires Failed	Remarks
40	9-7	92		
41	9-7	96		
42	9-10	96		
43	9-10	100	C-12	
44	9-11	100	B-12, C-2	TC 4 failed
45	9-11	100	C-5, D-9 & 10, F-11	
46	9-11	64	D-1 thru 12	Load aborted at 27 min
46a	9-12	100	C-0, D-11 & 12	
47	9-12	100		
48	9-13	104		
49	9-13	100		
50	9-13	96	D-4, 5 & 6, E-8	
51	9-17	54	C-2, 5 & 9, D-3, 4, 10 & 11, E-8 & 9	Load aborted at 24 min
52	9-17	43	B-9 & 10, D-2 & 9	Load aborted at 20 min
53	9-18	100	D-4, 5, 6, 7 & 8	
REPLACED ALL LOAD WIRES IN ROWS B THRU E				
54	9-19	100		
55	9-19	100		
56	9-19	100		
57	9-20	100		
58	9-20	48	D-1 thru 12	Load aborted at 22 min
59	9-20	100		
60	9-21	100		
REPLACED ALL LOAD WIRES IN ROW C				
61	9-21	100		
62	9-24	100		
63	9-24	37	B-9 & 10	Load aborted at 18 min
64	9-24	100		
65	9-25	100		
66	9-25	96		
67	9-25	100		
68	9-26	100		
69	9-26	100		
70	9-26	100		
71	9-27	100		
72	9-27	100		

**Table 5-1 Test Log (cont) (Sheet 3 of 3)**

Cycle	Date	% of Peak Hot Load Achieved	Loading Wires Failed	Remarks
73	9-27	54		Load aborted at 24 min
74	9-28	100		
75	9-28	100		
76	9-28	94		
77	10-1	100		
78	10-1	94		
79	10-1	96		
80	10-2	100		
81	10-2	96		
82	10-2	96		
83	10-3	100		
84	10-3	100		
85	10-3	100		
86	10-4	100		
87	10-4	100		
88	10-4	100		
FOUND LARGE CRACK ALONG CENTER OF PANEL; PHOTOGRAPHED CRACK; REPLACED 13 LOAD WIRES				
89	10-8	100		Load aborted at 24 min
90	10-8	55		
91	10-8	100		
92	10-9	100		
93	10-9	100		
94	10-9	100		
95	10-10	100		
96	10-10	100		
97	10-10	100		
98	10-11	100		
99	10-11	100		
100	10-11	100		



**Fig. 5-13 Surface Crack After 88 Cycles**

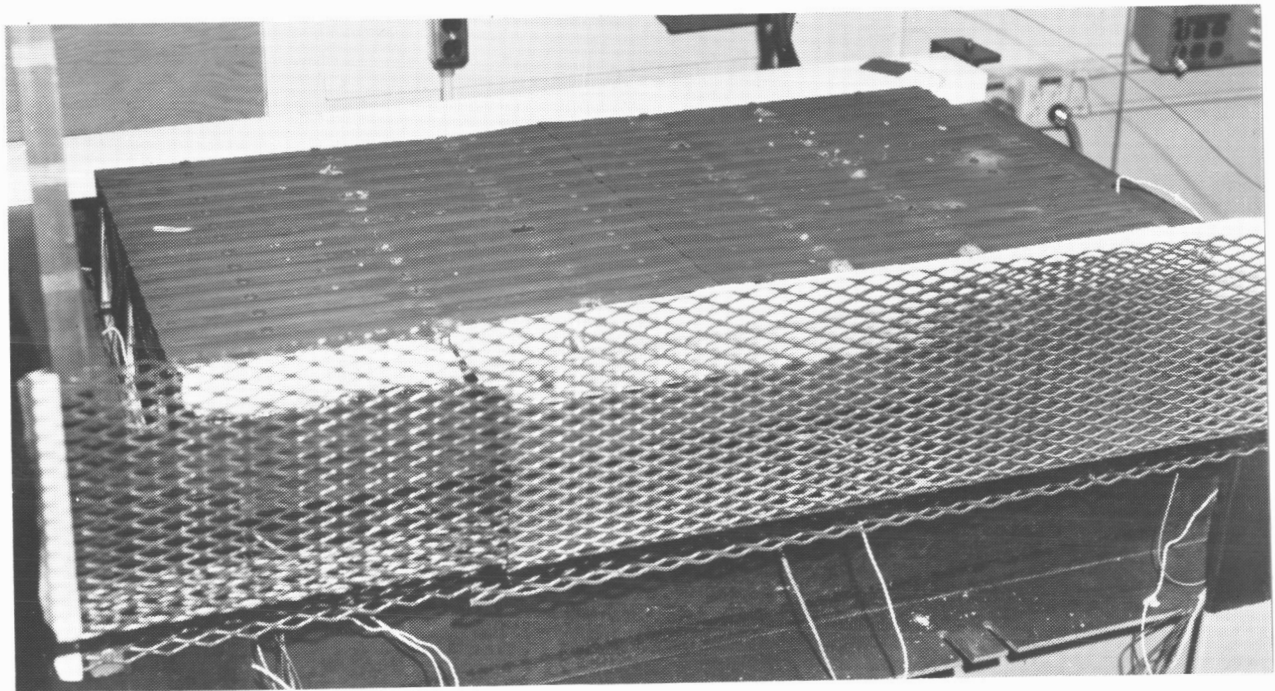


**Fig. 5-14 Test Article in Fixture After 100 Cycles**

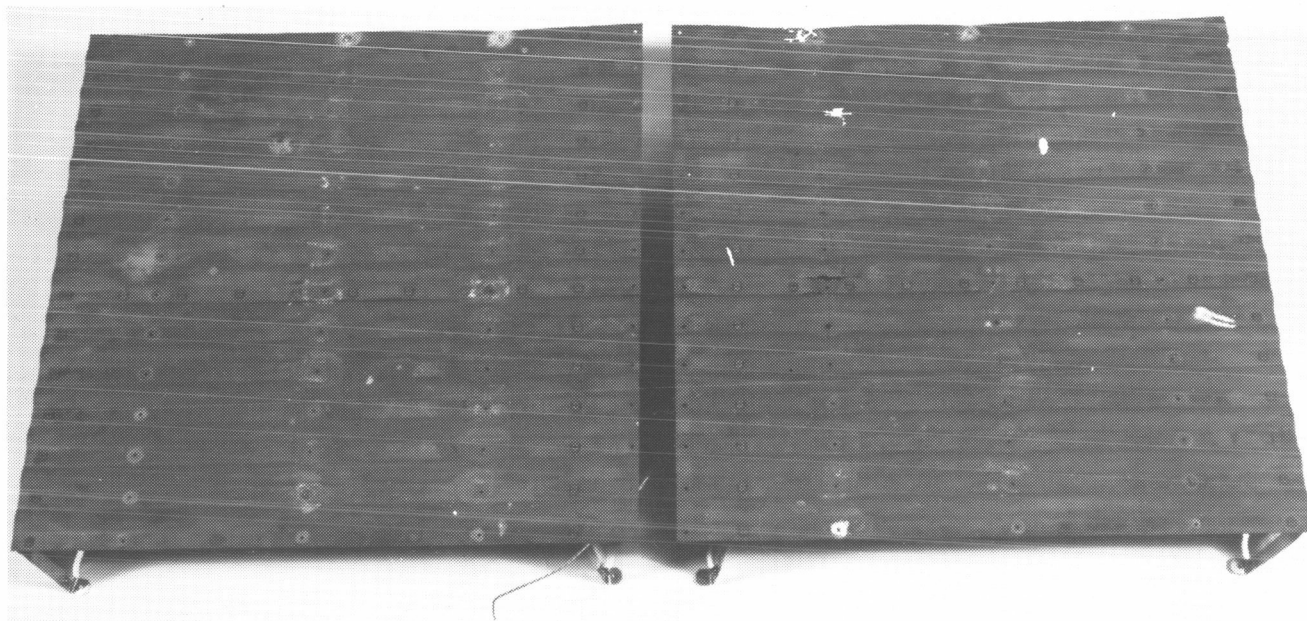


Fig. 5-15 Top Surface After 100 Cycles

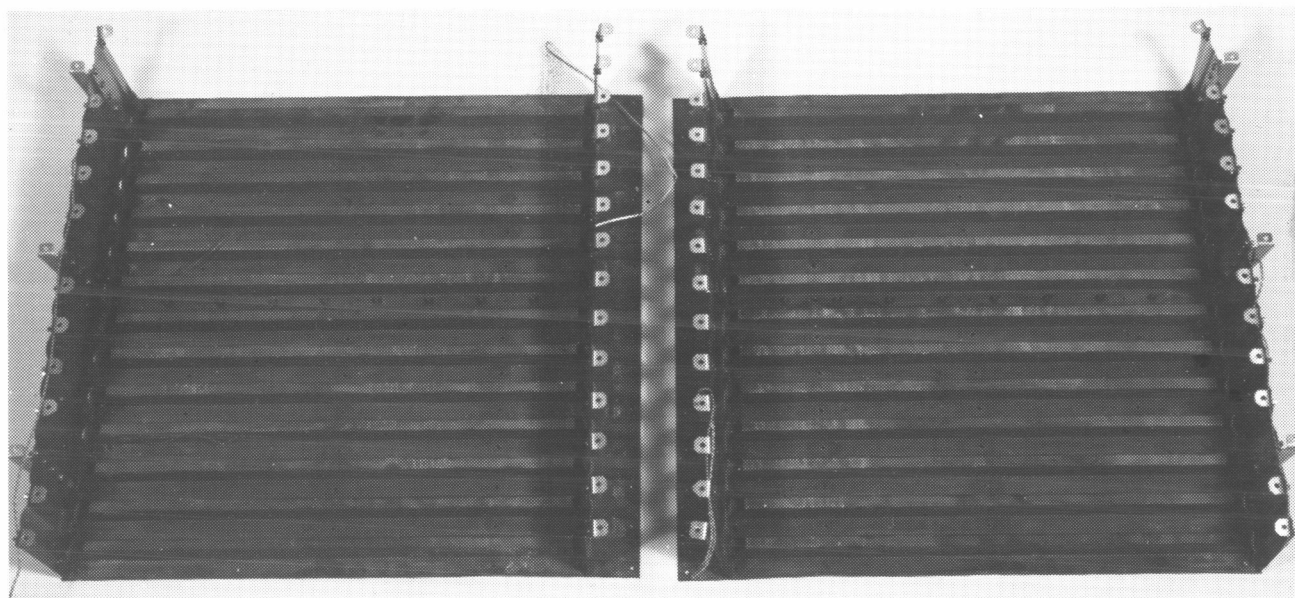


Fig. 5-16 Bottom Surface After 100 Cycles

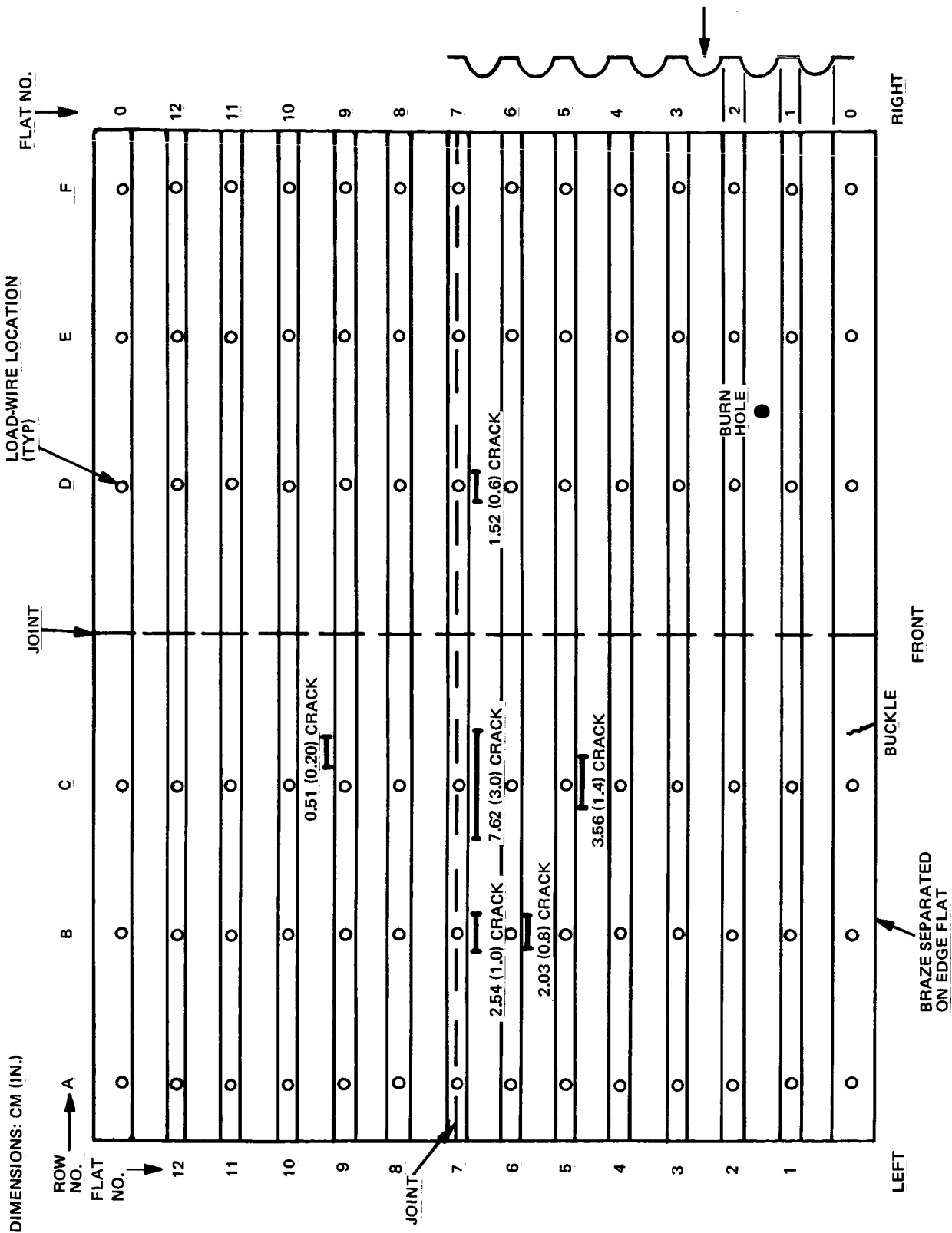
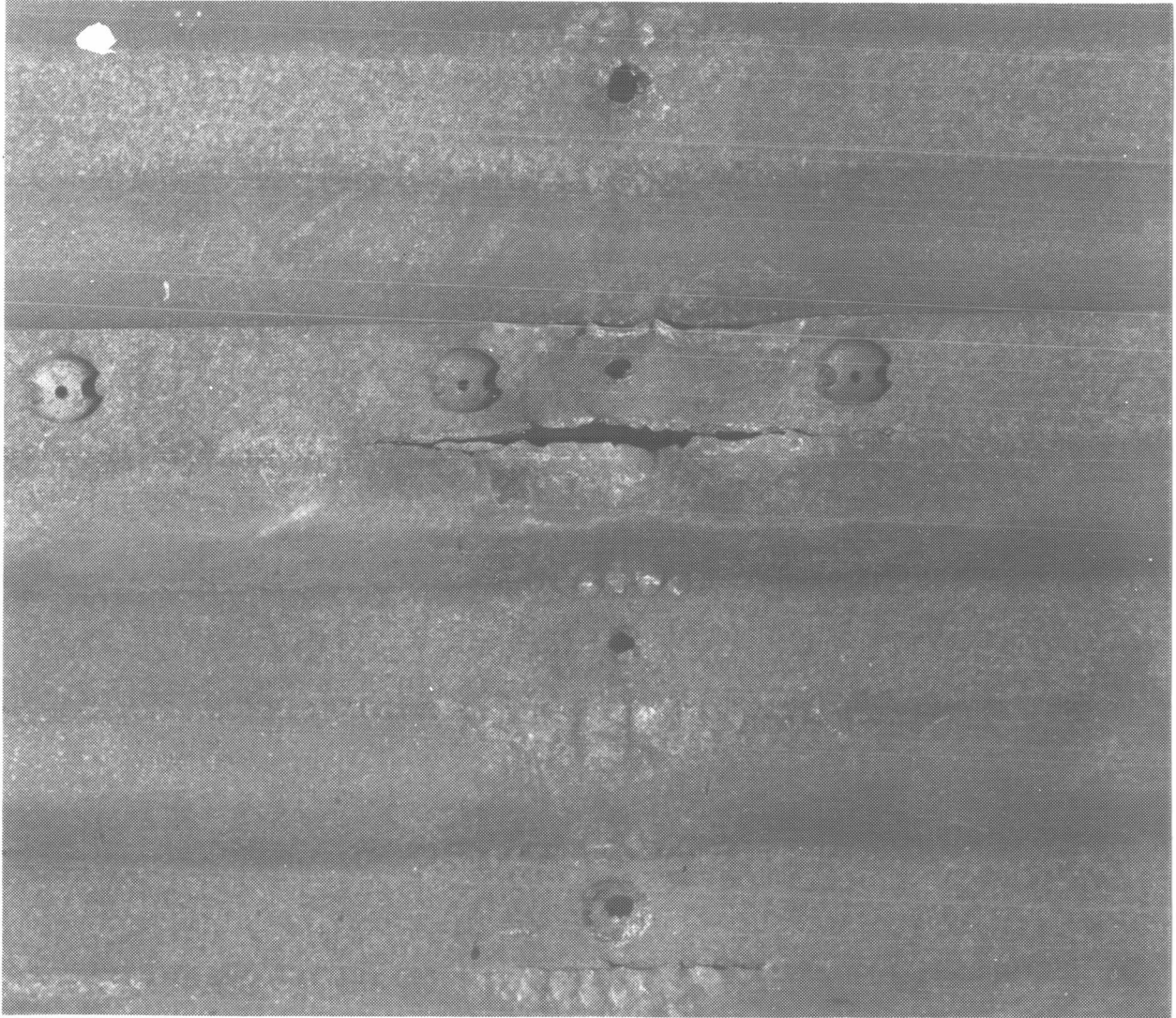
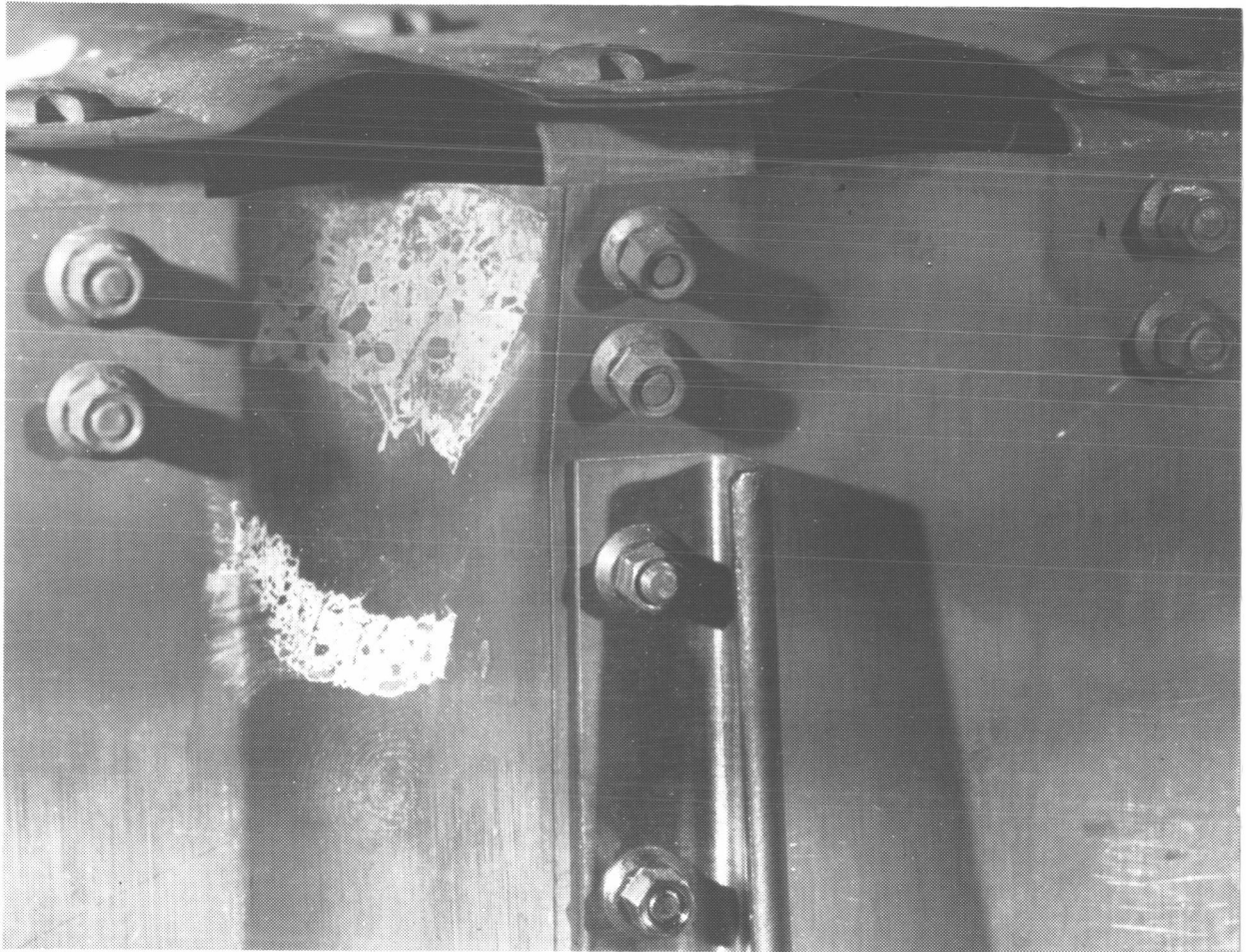


Fig. 5-17 Post-Test Inspection Surface Map, Run No. 100



**Fig. 5-18 Surface Cracks After 100 Cycles**



**Fig. 5-19 Kink in Support Rib**



Fig. 5-20 Insulation After 100 Cycles

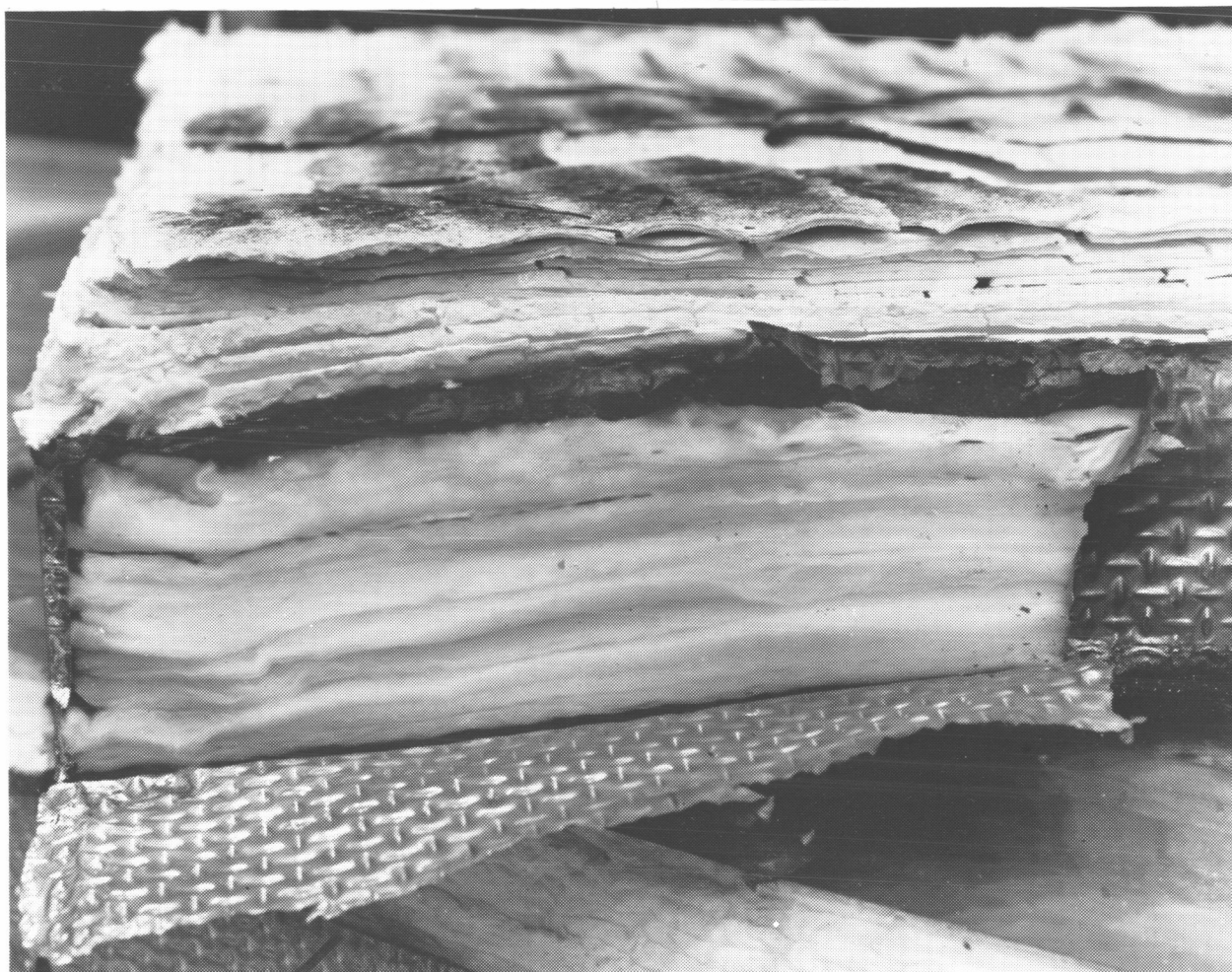


Fig. 5-21 Insulation After 100 Cycles

## Section 6

### CONCLUSIONS

The TD Ni-20Cr TPS panel completed 10 reentry temperature cycles, 90 launch and boost mechanical load cycles, and 90 combined temperature and pressure load reentry cycles. The following conclusions can be stated:

- The TD Ni-20Cr metallic panel was able to sustain design static loads and high temperature for 100 reentry cycles and also carry loads at room temperature between reentry cycles
- Creep and static load total deflection was 44% of allowable deflection
- The French-developed TD Ni-20Cr brazing process performed well
- The French-developed Protecator insulation system performed well and offers considerable weight advantage in the temperature range of 900-400°C (1650-750°F) over other commercially available insulations, pending proof of its ability to resist thermo-acoustic environments encountered in aerospace applications

## Section 7

### RECOMMENDATIONS FOR IMPROVED PANEL PERFORMANCE

Further development work that can improve the efficiency of this TPS approach should address the following:

- Optimization of the insulation. Increase peak temperature of the Protecator insulation to 900°C (1650°F). This will permit a removal of some of the higher-density Dynaflex. Also, take advantage of the reduced ambient pressure during reentry and its effect on reducing the thermal conductivity. This will further reduce the amount of insulation required
- Improvement in the design of the drag brackets of expansion joints to prevent kinking of the supports resulting from the horizontal loads
- A study to examine the fastening scheme in the longitudinal seam between panels to determine if the fasteners initiate cracks
- An improvement in the fastener design that will allow easy removal after cycling at 1200°C (2200°F)
- A study to determine if reduced atmospheric pressure and a flowing-air environment greatly alter the oxidation characteristics of TD Ni-20Cr at 1200°C (2200°F)
- An examination of the dynamic behavior of the panel after numerous thermal cycles, i.e., apply dynamic launch and boost and dynamic reentry loads in addition to static ones
- Develop a light-weight TD Ni-20Cr foil bagging

## Section 8

### REFERENCES

1. "Alternate Space Shuttle Concepts Study," B-35-43RP-12, Grumman Aerospace Corp., 6 July 1971.
2. "Proposal for Space Shuttle Program," 72-74 NAS, Grumman Aerospace Corp., 12 May 1972.
3. Sharp, D., "Minimum Weight Metallic Heat Shield," Shuttle Program Memo B35-197-M0-10, Grumman Aerospace Corp., 7 Oct 1970.
4. Sharp, D., "Material Choice for Lightest Metallic Heat Shield," Shuttle Program Memo B35-197-M0-11-A, Grumman Aerospace Corp., 21 Dec 1970.
5. Sharp, D., "TD Ni-Cr Heat Shield Weights," Shuttle Program Memo B35-197-M0-19, Grumman Aerospace Corp., 21 Jan 1971.
6. Ratay, R. T., and Fischer, W. E., "Development of A Reusable Metallic Thermal Protection System for Lifting Reentry Vehicles," Advanced Development Report No. ADR-01-04-70.1, Grumman Aerospace Corp., April 1970.
7. Harris, H. G., "Behavior of Full Size Metallic TPS Panels under Cyclic Reentry Environment," Presented at the Information Exchange on Creep of Materials for Space Shuttle Protection Systems, NASA Langley Research Center, 2-3 Dec 1971.
8. "Documentation and Analysis of Metallic Thermal Protection System (Haynes-25, Grumman Panel No. 4)," for NASA Langley Research Center Under Contract NAS 1-10925, Grumman Aerospace Corp., 1971.
9. "Stress Report, Aeroelastic Test Program, Test Cavity and Test Panels," for NASA Langley Research Center Under Contract NAS 1-10635-1, Grumman Aerospace Corp., 1972.

10. Ojalvo, I. U., and Arcas, N., "Approximate Analysis and Dynamic Test for a TPS Panel," Presented at the NASA Space Shuttle Technology Conference, NASA Langley Research Center, 2-4 March 1971.
11. Morman, K. N., "Correlation of Theoretical TPS Creep Deflections with Test Results," Presented at the Information Exchange on Creep of Materials for Space Shuttle Protection Systems, NASA Langley Research Center, 2-3 Dec 1971.
12. "Programmes de Recherche sur des Rivetment Metallique a Haute Temperature et sur des Insulation Thermique Non-consumable," AMD Document DGT No. 6528, Parts I and II, Avions Marcel Dassault, St. Cloud, France, 1 Dec 1971.
13. "Etude d'un Matelas d'Insolation Thermique," AMD Document No. 8262, Avions Marcel Dassault, St. Cloud, France, 13 July 1972.
14. Picard, C., and Chaumette, D., "Research Work in the Space Shuttle Technology Field," AMD Document No. 7663, Avions Marcel Dassault, St. Cloud, France, 10 Jan 1972.
15. Klingler, L. J., Weinberger, W. R., Bailey, P. G., and Baranow, S.: "Development of Dispersion-Strengthened Nickel-Chromium Alloy (Ni-Cr-THO<sub>2</sub>) Sheet for Space Shuttle Vehicles," NASA CR-120796, Dec 1971.
16. Johnson, Jr., R., and Killpatrick, D. H.: "Dispersion-Strengthened Metal Structural Development," AFFDL-TR-68-130, Part I (1968), Part II (1973).
17. Fritz, L. J.: "Characterization of Mechanical and Physical Properties of TD Ni-Cr (Ni-20Cr-2THO<sub>2</sub>) Alloy," Contract NAS 3-15558, Monthly Reports 1 (7 July 1971) through 15 (1 Oct 1972).
18. Johnson, Jr., R., and Killpatrick, D. H.: "Evaluation of Dispersion-Strengthened Nickel-Base Alloy Heat Shields for Space Shuttle Application," NASA CR-132360, May 1973.

19. Holko, K.H.: "TD Ni-Cr Sheet - Mechanical and Physical Properties, Welding and Forming - State-of-Technology Report," NASA TMX-52952, Jan 1971.
20. Giggins, C. S., and Pettit, F. S.: "The Oxidation of TD Ni-Cr (Ni-20Cr-2 Vol pct THO<sub>2</sub>) Between 900 and 1200<sup>o</sup>C," Metallurgical Transactions, Vol 2, pages 1071-78, April 1971.

## Appendix

### FLATNESS SURVEY DATA

Presented here are the load-deflection survey data and the flatness survey data taken after cycles 10, 19, 40, 50, 60, 80, and 100. Figure A-1 shows the locations of the various points where the dial indicator deflection data were taken. These points are described by the same numbering system as the loading wires; the points differ in location only in that they are shifted 1.3 cm (0.5 in.) to the left of the load points.

The data in Tables A-1 through A-8 are the changes in vertical height of the measurement points, with positive numbers being downward. The accuracy of these measurements is approximately  $\pm 0.003$  in.

**Fig. A-1 Flatness Survey Location Map**

Table A-1 Load-Deflection Survey, Flat No. 7

CHANGE (IN.) FROM ZERO LOAD

Load, lb	Dial Indicator No. (Left to Right)						
	1	2	3	4	5	6	7
0	0	0	0	0	0	0	0
100	0.029	0.026	0.017	0.001	0.008	0.011	0.008
200	0.038	0.041	0.028	0.002	0.016	0.023	0.016
300	0.046	0.055	0.040	0.004	0.024	0.035	0.025
400	0.054	0.067	0.052	0.004	0.032	0.047	0.033
500	0.063	0.083	0.063	0.006	0.040	0.058	0.040
600	0.070	0.096	0.073	0.006	0.047	0.069	0.048
700	0.079	0.111	0.084	0.006	0.055	0.080	0.055
800	0.086	0.124	0.094	0.006	0.062	0.090	0.062
900	0.094	0.137	0.104	0.007	0.070	0.101	0.069
965	0.099	0.145	0.110	0.007	0.074	0.108	0.073
0	0.022	0.016	0.009	0.003	0.001	0.002	0.002

Table A-2 Flatness Survey No. 2, After Cycle No. 10

CHANGE (IN.) FROM FLATNESS SURVEY NO. 1

Flat No.	Dial Indicator No. (Left to Right)						
	1	2	3	4	5	6	7
1	-0.004	0.007	0.013	0.020	0.006	0.004	0.000
2	-0.002	0.011	0.020	0.032	0.016	0.012	0.009
3	0.009	0.024	0.035	0.046	0.027	0.022	0.017
4	0.016	0.029	0.038	0.050	0.034	0.028	0.023
5	0.020	0.031	0.042	0.056	0.038	0.033	0.027
6	0.020	0.031	0.044	0.063	0.074	0.037	0.031
7	0.007	0.022	0.036	0.044	0.038	0.030	0.026
8	0.019	0.031	0.042	0.056	0.039	0.030	0.025
9	0.015	0.026	0.037	0.049	0.032	0.024	0.021
10	0.011	0.020	0.036	0.050	0.032	0.030	0.026
11	-0.002	0.012	0.021	0.032	0.012	0.008	0.007
12	-0.017	0.001	0.004	0.009	0.001	-0.003	-0.004

Table A-3 Flatness Survey No. 3, After Cycle No. 19

CHANGE (IN.) FROM FLATNESS SURVEY NO. 1

Flat No.	Dial Indicator No. (Left to Right)						
	1	2	3	4	5	6	7
1	0.001	0.012	-0.004	-0.065	-0.029	-0.016	-0.015
2	0.014	0.018	0.005	-0.016	-0.017	-0.005	-0.004
3	0.025	0.036	0.024	0.003	0.000	0.009	0.009
4	0.032	0.043	0.032	0.014	0.011	0.019	0.018
5	0.037	0.045	0.034	0.024	0.017	0.026	0.025
6	0.037	0.045	0.039	0.036	0.026	0.034	0.031
7	0.029	0.048	0.037	0.006	0.024	0.030	0.028
8	0.044	0.065	0.043	0.027	0.027	0.032	0.031
9	0.044	0.054	0.043	0.023	0.021	0.028	0.027
10	0.038	0.043	0.033	0.012	0.009	0.022	0.023
11	0.028	0.029	0.023	0.002	-0.002	0.010	0.012
12	0.011	0.021	0.006	-0.021	-0.015	-0.001	0.001

Table A-4 Flatness Survey No. 4, After Cycle No. 40

CHANGE (IN.) FROM FLATNESS SURVEY NO. 1

Flat No.	Dial Indicator No. (Left to Right)						
	1	2	3	4	5	6	7
1	0.010	0.027	0.009	-0.034	-0.024	-0.008	-0.009
2	0.013	0.028	0.013	-0.013	-0.009	0.004	0.003
3	0.033	0.045	0.031	0.007	0.006	0.015	0.014
4	0.037	0.049	0.037	0.021	0.020	0.030	0.030
5	0.040	0.048	0.035	0.026	0.022	0.032	0.031
6	0.039	0.047	0.037	0.037	0.030	0.040	0.037
7	0.032	0.045	0.037	-0.001	0.030	0.034	0.033
8	0.049	0.063	0.049	0.025	0.030	0.036	0.034
9	0.048	0.062	0.048	0.022	0.024	0.031	0.031
10	0.041	0.045	0.035	0.010	0.009	0.023	0.025
11	0.029	0.040	0.024	-0.001	0.000	0.010	0.013
12	0.013	0.024	0.008	-0.026	-0.015	0.000	0.002

Table A-5 Flatness Survey No. 5, After Cycle No. 50

CHANGE (IN.) FROM FLATNESS SURVEY NO. 1

Flat No.	Dial Indicator No. (Left to Right)						
	1	2	3	4	5	6	7
1	0.013	0.035	0.018	-0.032	-0.016	-0.001	-0.006
2	0.012	0.030	0.016	-0.013	-0.006	0.008	0.006
3	0.032	0.046	0.032	0.007	0.006	0.017	0.015
4	0.037	0.049	0.038	0.017	0.013	0.026	0.025
5	0.039	0.051	0.040	0.026	0.023	0.035	0.032
6	0.041	0.050	0.042	0.037	0.034	0.035	0.041
7	0.043	0.050	0.108	0.005	0.036	0.039	0.037
8	0.052	0.067	0.046	0.025	0.035	0.042	0.037
9	0.051	0.067	0.051	0.022	0.030	0.037	0.034
10	0.043	0.052	0.046	0.012	0.014	0.033	0.032
11	0.033	0.042	0.057	0.002	0.004	0.017	0.017
12	0.015	0.028	0.061	-0.026	-0.010	0.005	0.004

Table A-6 Flatness Survey No. 6, After Cycle No. 60

CHANGE (IN.) FROM FLATNESS SURVEY NO. 1

Flat No.	Dial Indicator, No. (Left to Right)						
	1	2	3	4	5	6	7
1	0.022	0.049	0.041	-0.046	-0.017	-0.002	-0.006
2	0.013	0.034	0.023	-0.013	-0.007	0.006	0.004
3	0.033	0.049	0.038	0.009	0.009	0.019	0.016
4	0.038	0.052	0.043	0.019	0.020	0.028	0.024
5	0.048	0.007	0.040	0.027	0.026	0.035	0.032
6	0.040	0.053	0.045	0.036	0.032	0.041	0.039
7	0.033	0.052	0.046	-0.006	0.032	0.035	0.036
8	0.047	0.070	0.059	0.025	0.034	0.038	0.036
9	0.052	0.066	0.053	0.022	0.029	0.035	0.033
10	0.045	0.055	0.045	0.012	0.014	0.031	0.032
11	0.032	0.045	0.029	-0.001	0.002	0.015	0.016
12	0.017	0.031	0.014	-0.024	-0.010	0.004	0.005

Table A-7 Flatness Survey No. 7, After Cycle No. 80

CHANGE (IN.) FROM FLATNESS SURVEY NO. 1

Flat No.	Dial Indicator No. (Left to Right)						
	1	2	3	4	5	6	7
1	0.025	0.056	0.050	-0.044	-0.012	0.002	-0.003
2	0.016	0.043	0.032	-0.012	-0.002	0.009	0.006
3	0.035	0.061	0.043	0.010	0.013	0.022	0.019
4	0.040	0.063	0.050	0.022	0.028	0.035	0.034
5	0.041	0.058	0.051	0.026	0.032	0.036	0.035
6	0.040	0.057	0.055	0.034	0.037	0.043	0.041
7	0.035	0.060	0.053	-0.007	0.014	0.022	0.038
8	0.057	0.070	0.073	0.026	0.039	0.041	0.037
9	0.056	0.085	0.069	0.021	0.036	0.039	0.026
10	0.051	0.070	0.061	0.018	0.019	0.042	0.044
11	0.037	0.053	0.040	0.002	0.008	0.017	0.016
12	0.121	0.038	0.024	-0.021	-0.005	0.006	0.005

Table A-8 Flatness Survey No. 8, After Cycle No. 100

CHANGE (IN.) FROM FLATNESS SURVEY NO. 1

Flat No.	Dial Indicator No. (Left to Right)						
	1	2	3	4	5	6	7
1	0.029	0.070	0.071	-0.040	-0.007	0.001	0.008
2	0.017	0.053	0.042	-0.009	0.001	0.009	0.013
3	0.037	0.071	0.059	0.013	0.015	0.022	0.025
4	0.048	0.067	0.064	0.024	0.031	0.035	0.038
5	0.045	0.073	0.075	0.027	0.037	0.040	0.042
6	0.045	0.074	0.075	0.031	0.043	0.048	0.050
7	0.040	0.074	0.063	-0.008	-0.031	0.011	0.047
8	0.058	0.062	0.082	0.023	0.050	0.051	0.047
9	0.058	0.097	0.071	0.022	0.043	0.049	0.044
10	0.051	0.079	0.066	0.013	0.002	0.039	0.040
11	0.038	0.061	0.049	0.006	0.016	0.027	0.028
12	0.022	0.046	0.034	-0.017	0.006	0.014	0.017